

The hyperonic star in relativistic mean-field model

Kaixuan Huang, Jinniu Hu,^{*} and Hong Shen[†]

School of Physics, Nankai University, Tianjin 300071, China

Ying Zhang[‡]

Department of Physics, School of Science,

Tianjin University, Tianjin 300072, China

(Dated: March 24, 2022)

Abstract

The neutron star as a supernova remnant is attracting high attention recently due to the gravitation wave detection and precise measurements about its mass and radius. In the inner core region of the neutron star, the strangeness degrees of freedom, such as the hyperons, can be present, which is also named as a hyperonic star. In this work, the neutron star consisting of nucleons and leptons, and the hyperonic star including the hyperons will be reviewed in the framework of the relativistic mean-field (RMF) model. The popular non-linear and density-dependent RMF parametrizations in the market will be adopted to investigate the role of strangeness baryons in a hyperonic star on its mass, radius, tidal deformability, and other properties. Finally, the magnitudes of the coupling strengths between mesons and hyperons also will be discussed, which can generate the massive hyperonic star with present RMF parameter sets, when the vector coupling constants are strong.

PACS numbers: 21.10.Dr, 21.60.Jz, 21.80.+a

^{*} hujinniu@nankai.edu.cn

[†] songtc@nankai.edu.cn

[‡] yzhangjcnp@tju.edu.cn

I. INTRODUCTION

The star, whose mass is in the range of $8M_{\odot} \sim 20M_{\odot}$, will undergo a supernova explosion at the end of its life. The remnant may form a very compact object mainly consisting of nucleons and leptons, i.e., neutron stars. Due to the strong magnetic field ($B \sim 10^{11} - 10^{15}$ G) and fast rotation of neutron star ($P \sim 10^{-3} - 10$ s), it can emit the beam of electromagnetic radiation from the magnetic poles, which was detected from the earth as a pulsar. In the past 50 years, more than 3000 pulsars were measured, whose typical masses are around $1 \sim 2M_{\odot}$ and radii are about 10 km. Therefore, the neutron star should consist of very dense matter. Its central density is close to $5 - 8\rho_0$, where $\rho_0 \sim 0.16 \text{ fm}^{-3}$ is the nuclear saturation density. It is difficult to investigate the properties of such supra-dense matter in the terrestrial nuclear laboratory until now [1–10].

There were many great achievements in the observations of the neutron star in the past decade with the fast developments of astronomical techniques. Several massive neutron stars, whose masses are around $2M_{\odot}$, PSR J1614-2230 ($1.928 \pm 0.017M_{\odot}$) [11–13], PSR J0348+0432 ($2.01 \pm 0.04M_{\odot}$) [14], and PSR J0740+6620 ($2.08 \pm 0.07M_{\odot}$) [15, 16] were measured within the relativistic Shapiro delay effect. In the August of 2017, the gravitational wave and the electromagnetic counterpart of a binary neutron-star merger were detected by LIGO/Virgo and other astronomical observatories for the first time as GW170817 event [17–19]. It opens the door to the multi-messenger astronomy era. From the gravitational wave, the tidal deformability of the neutron star is extracted, which is strongly correlated with the structures of the neutron star. Five gravitational wave events which are relevant to the neutron star have been detected until now, i.e. GW170817, GW190425 [20], GW190814 [21], GW200105, and GW200115 [22]. The masses of these compact objects are in a wide region from $0.86M_{\odot}$ to $2.67M_{\odot}$ [23]. The dimensionless tidal deformability of $1.4M_{\odot}$ neutron star extracted from GW170817 was 190_{-120}^{+390} [24–26].

The structure of a static neutron star is separated into five regions. The outer layer is the atmosphere consisting of the atom and is very thin. In the next layer as the outer crust, the electrons of an atom are ionized and form the uniform Fermi gas, where the nuclei are immersed. With the density increasing, neutrons drip out from the neutron-rich nuclei and generate the neutron gas, which is called the inner crust. The inhomogeneous nuclear matter is simplified as the droplet, rod, slab, tube, and bubble, i.e. the pasta structure [27–

36]. When the nucleon density approaches $\rho_0/2$, heavy nuclei dissolve and the neutron star matter becomes homogeneous, which corresponds to the outer core of neutron star. It plays an essential role in determining the mass and radius of the neutron star [37–41]. In the inner core region, the baryons including the strangeness degree of freedom, such as Λ , Σ , and Ξ hyperons, will be present, when the Fermi energies of nucleons are larger than their chemical potentials, which is also called as a hyperonic star. Furthermore, the quarks in the baryons are deconfined and generate quark matter [42–58].

In 1960, Ambartsumyan and Saakyan firstly discussed the appearances of various hyperons in the free dense matter through the chemical equilibrium conditions [59]. The hyperons were investigated in neutron stars from the 1980s by Glendenning in the framework of relativistic mean-field (RMF) model, where the coupling strengths between the mesons and baryons were simply generated by the quark power counting rules [60, 61]. Actually, the appearances of hyperons are strongly dependent on the hyperon-nucleon and hyperon-hyperon potentials, which can be extracted from the properties of various hypernuclei. Recently, an abundant single- Λ hypernuclei were produced through (K^-, π^-) , (π^+, K^+) , and $(e, e'K^+)$ reactions from light to heavy mass regions [62–65]. A few double- Λ hypernuclei were discovered in the light nuclei [66, 67] and the first deep bound state of single- Ξ hypernuclei was confirmed in the $\Xi^- + {}^{14}\text{N}$ (${}^{15}_{\Xi^-}\text{C}$) system [68–70]. The observations of these hypernuclei imply that the Λ -nucleon and Ξ -nucleon potentials in nuclear medium should be attractive around nuclear saturation density [71, 72].

In the past 30 years, the RMF parametrizations about nucleon-nucleon and nucleon-hyperon interactions were largely improved through reproducing the ground-state properties of finite nuclei and above hypernuclei experimental data, that were adopted to investigate the hyperonic star [73–86]. On the other hand, the strangeness degree of freedom in the neutron star was also discussed directly from the realistic baryon-baryon interactions with *ab initio* methods, such as Brueckner Hartree-Fock model [87–93], auxiliary field diffusion Monte Carlo model [94], relativistic Brueckner-Hartree-Fock model, and so on [95, 96].

With the discoveries of two-times-solar-mass neutron stars, a “hyperon puzzle” was proposed, since the neutron star maximum mass will be reduced by about 20% once the hyperons are self-consistently introduced in the nuclear many-body methods. Therefore, it is difficult to explain the existence of massive neutron stars with hyperons at the beginning. Many schemes were raised to solve such a puzzle. The repulsive contributions from three-body

hyperon-nucleon-nucleon interaction may increase the hyperonic star mass [92–94]. A high-density σ -cut potential can generate $2M_{\odot}$ neutron stars with Λ , Σ , and Ξ hyperons in the relativistic mean-field model [81]. Furthermore, the density-dependent RMF (DDRMF) model under the constraints of Λ hypernuclei also can support the massive hyperonic star due to its strong repulsive components on the pressure at high density [97]. Recently, the role of vector meson including the strange quark, ϕ was also discussed in the hyperonic star with various hyperons [85].

In this paper, the hyperonic star in the framework of RMF and DDRMF models will be systematically calculated with the most popular parameterizations. The exchange mesons with strangeness quarks will be completely included in RMF framework. The coupling strengths between the mesons and baryons will be constrained with the latest hypernuclei experimental data. The effects of their magnitudes on the properties of hyperonic stars are discussed in the last part. This paper is arranged as follows. In Section 2, the formulas about the neutron star and hyperonic star with the RMF model are shown in detail. In Section 3, the parametrizations of the nonlinear RMF and DDRMF model are listed and the properties of neutron stars and hyperonic stars are calculated and discussed. In Section 4, the summary and conclusion will be given.

II. THEORETICAL FRAMEWORK

A. The nonlinear Relativistic Mean-field Model

The relativistic mean-field (RMF) model was constructed based on the one-boson-exchange picture for the nucleon-nucleon (NN) interaction. In the early version, there were only scalar (σ) and vector mesons (ω), which present the attractive and repulsive components of NN interaction, respectively [98]. Then, the nonlinear terms of σ meson were introduced to reduce the incompressibility of nuclear matter [99]. The isovector meson, ρ was introduced to correctly describe the neutron star matter [100]. The nonlinear term of ω meson [101] and the coupling terms between the ω and ρ mesons [102] were also included to improve the high-density behaviors of nuclear matter and density-dependence of symmetry energy, respectively. Furthermore, a density-dependent RMF (DDRMF) model [103] was proposed based on the developments of relativistic Brueckner-Hartree-Fock (RBHF)

model. When the masses of exchanging mesons are regarded as infinite, the NN interaction is simplified as contact potential, which generates the point-coupling RMF (PCRMF) models [104].

In the nonlinear RMF (NLRMF) model, the baryons interact with each other via exchanging various light mesons, including scalar-isoscalar meson (σ), vector-isoscalar meson (ω), vector-isovector meson (ρ), and strange scalar and vector mesons (σ^* and ϕ) [105–110]. The baryons considered in the present calculation are nucleons (n and p) and hyperons (Λ , Σ , Ξ). The Lagrangian density of NLRMF model is written as

$$\begin{aligned}
\mathcal{L}_{\text{NL}} = & \sum_B \bar{\psi}_B \left\{ i\gamma^\mu \partial_\mu - (M_B - g_{\sigma B}\sigma - g_{\sigma^* B}\sigma^*) \right. \\
& \left. - \gamma^\mu \left(g_{\omega B}\omega_\mu + g_{\phi B}\phi_\mu + \frac{1}{2}g_{\rho B}\vec{\rho}_\mu \right) \right\} \psi_B \\
& + \frac{1}{2}\partial^\mu\sigma\partial_\mu\sigma - \frac{1}{2}m_\sigma^2\sigma^2 - \frac{1}{3}g_2\sigma^3 - \frac{1}{4}g_3\sigma^4 \\
& + \frac{1}{2}\partial^\mu\sigma^*\partial_\mu\sigma^* - \frac{1}{2}m_{\sigma^*}^2\sigma^{*2} \\
& - \frac{1}{4}W^{\mu\nu}W_{\mu\nu} + \frac{1}{2}m_\omega^2\omega^\mu\omega_\mu + \frac{1}{4}c_3(\omega^\mu\omega_\mu)^2 \\
& - \frac{1}{4}\Phi^{\mu\nu}\Phi_{\mu\nu} + \frac{1}{2}m_\phi^2\phi^\mu\phi_\mu \\
& - \frac{1}{4}\vec{R}^{\mu\nu}\vec{R}_{\mu\nu} + \frac{1}{2}m_\rho^2\vec{\rho}^\mu\vec{\rho}_\mu \\
& + \Lambda_v(g_\omega^2\omega^\mu\omega_\mu)(g_\rho^2\vec{\rho}^\mu\vec{\rho}_\mu),
\end{aligned} \tag{1}$$

where ψ_B represents the wave function of baryons. σ , σ^* , ω_μ , ϕ_μ , $\vec{\rho}_\mu$ denote the fields of σ , σ^* , ω , ϕ , and ρ mesons, respectively. $W_{\mu\nu}$, $\Phi_{\mu\nu}$, and $\vec{R}_{\mu\nu}$ are the anti-symmetry tensor fields of ω , ϕ , and ρ mesons. Here $g_{\omega B}$ denotes the coupling constant between ω meson and baryon, while g_ω for the coupling strength between ω meson and nucleon. To solve the nuclear many-body system in the framework of the NLRMF model, the mean-field approximation should be adopted, in which various mesons are treated as classical fields,

$$\begin{aligned}
\sigma & \rightarrow \langle\sigma\rangle \equiv \sigma, \quad \sigma^* \rightarrow \langle\sigma^*\rangle \equiv \sigma^*, \\
\omega_\mu & \rightarrow \langle\omega_\mu\rangle \equiv \omega, \quad \phi_\mu \rightarrow \langle\phi_\mu\rangle \equiv \phi, \\
\vec{\rho}_\mu & \rightarrow \langle\vec{\rho}_\mu\rangle \equiv \rho.
\end{aligned} \tag{2}$$

The space components of the vector mesons are removed in the parity conservation system. In addition, the spatial derivatives of baryons and mesons are neglected in the infinite nuclear matter due to the transformation invariance. Finally, with the Euler-Lagrange equation, the

equations of motion for baryons and mesons are obtained,

$$\begin{aligned}
& \left[i\gamma^\mu \partial_\mu - M_B^* - \gamma^0 \left(g_{\omega B} \omega + g_{\phi B} \phi + \frac{g_{\rho B}}{2} \rho \tau_3 \right) \right] \psi_B = 0, \\
& m_\sigma^2 \sigma + g_2 \sigma^2 + g_3 \sigma^3 = \sum_B g_{\sigma B} \rho_B^s, \\
& m_{\sigma^*}^2 \sigma^* = \sum_B g_{\sigma^* B} \rho_B^s, \\
& m_\omega^2 \omega + c_3 \omega^3 + 2\Lambda_v (g_\omega^2 \omega) (g_\rho^2 \rho^2) = \sum_B g_{\omega B} \rho_B^v, \\
& m_\phi^2 \phi = \sum_B g_{\phi B} \rho_B^v, \\
& m_\rho^2 \rho + 2\Lambda_v (g_\omega^2 \omega^2) (g_\rho^2 \rho) = \sum_B \frac{g_{\rho B}}{2} \rho_B^{v3},
\end{aligned} \tag{3}$$

where τ_3 is the isospin third component of the baryon species B . The scalar (s), vector densities (v), and their isospin components are defined as,

$$\begin{aligned}
\rho_B^s &= \langle \bar{\psi}_B \psi_B \rangle, & \rho_B^{s3} &= \langle \bar{\psi}_B \tau_3 \psi_B \rangle, \\
\rho_B^v &= \langle \psi_B^\dagger \psi_B \rangle, & \rho_B^{v3} &= \langle \psi_B^\dagger \tau_3 \psi_B \rangle.
\end{aligned} \tag{4}$$

The effective masses of baryons in Eq. (3) are dependent on the scalar mesons σ and σ^* ,

$$M_B^* = M_B - g_{\sigma B} \sigma - g_{\sigma^* B} \sigma^*. \tag{5}$$

The corresponding effective energies of baryons take the following form because of the mass-energy relation,

$$E_{FB}^* = \sqrt{k_{FB}^2 + (M_B^*)^2}, \tag{6}$$

where k_{FB} is the Fermi momentum of baryons.

With the energy-momentum tensor in a uniform system, the energy density, \mathcal{E} and pres-

sure, P of infinite nuclear matter are obtained respectively as [108]

$$\begin{aligned}
\mathcal{E}_{\text{NL}} = & \frac{\gamma}{16\pi^2} \sum_B \left[k_{FB} E_{FB}^* (2k_{FB}^2 + M_B^{*2}) \right. \\
& \left. + M_B^{*4} \ln \frac{M_B^*}{k_{FB} + E_{FB}^*} \right] \\
& + \frac{1}{2} m_\sigma^2 \sigma^2 + \frac{1}{3} g_2 \sigma^3 + \frac{1}{4} g_3 \sigma^4 + \frac{1}{2} m_{\sigma^*}^2 \sigma^{*2} \\
& + \frac{1}{2} m_\omega^2 \omega^2 + \frac{3}{4} c_3 \omega^4 + \frac{1}{2} m_\rho^2 \rho^2 + 3\Lambda_\nu (g_\omega^2 \omega^2) (g_\rho^2 \rho^2), \tag{7}
\end{aligned}$$

$$\begin{aligned}
P_{\text{NL}} = & \frac{\gamma}{48\pi^2} \sum_B \left[3M_B^{*4} \ln \frac{k_{FB} + E_{FB}^*}{M_B^*} \right. \\
& \left. + k_{FB}^2 (2k_{FB}^2 - 3M_B^{*2}) E_{FB}^* \right] \\
& - \frac{1}{2} m_\sigma^2 \sigma^2 - \frac{1}{3} g_2 \sigma^3 - \frac{1}{4} g_3 \sigma^4 - \frac{1}{2} m_{\sigma^*}^2 \sigma^{*2} \\
& + \frac{1}{2} m_\omega^2 \omega^2 + \frac{c_3}{4} \omega^4 + \frac{1}{2} m_\rho^2 \rho^2 + \Lambda_\nu (g_\omega^2 \omega^2) (g_\rho^2 \rho^2). \tag{8}
\end{aligned}$$

where $\gamma = 2$ is the spin degeneracy factor.

The outer core part of a neutron star, which almost dominates its mass and radius, is usually treated as the uniform matter consisting of baryons and leptons. Therefore their chemical potentials are very important, that are derived from the thermodynamics equations at zero temperature,

$$\begin{aligned}
\mu_B = & \sqrt{k_{FB}^2 + M_B^{*2}} + g_{\omega B} \omega + g_{\phi B} \phi + \frac{g_{\rho B}}{2} \tau_3 \rho, \\
\mu_l = & \sqrt{k_{Fl}^2 + m_l^2}, \quad l = e, \mu. \tag{9}
\end{aligned}$$

B. The Density-dependent Relativistic Mean-field Model

In the DDRMF model, the Lagrangian density of nuclear many-body system has the similar form as that of NLRMF model,

$$\begin{aligned}
\mathcal{L}_{\text{DD}} = & \sum_B \bar{\psi}_B \left[\gamma^\mu (i\partial_\mu - \Gamma_{\omega B}(\rho_B)\omega_\mu \right. \\
& \left. - \Gamma_{\phi B}(\rho_B)\phi_\mu - \frac{\Gamma_{\rho B}(\rho_B)}{2}\vec{\rho}_\mu\vec{\tau} \right) \\
& - \left(M_B - \Gamma_{\sigma B}(\rho_B)\sigma - \Gamma_{\sigma^* B}(\rho_B)\sigma^* - \Gamma_{\delta B}(\rho_B)\vec{\delta}\vec{\tau} \right) \Big] \psi_B \\
& + \frac{1}{2} (\partial^\mu\sigma\partial_\mu\sigma - m_\sigma^2\sigma^2) + \frac{1}{2} (\partial^\mu\sigma^*\partial_\mu\sigma^* - m_{\sigma^*}^2\sigma^{*2}) \\
& + \frac{1}{2} (\partial^\mu\vec{\delta}\partial_\mu\vec{\delta} - m_\delta^2\vec{\delta}^2) - \frac{1}{4} W^{\mu\nu}W_{\mu\nu} + \frac{1}{2} m_\omega^2\omega_\mu\omega^\mu \\
& - \frac{1}{4} \Phi^{\mu\nu}\Phi_{\mu\nu} + \frac{1}{2} m_\phi^2\phi_\mu\phi^\mu - \frac{1}{4} \vec{R}^{\mu\nu}\vec{R}_{\mu\nu} + \frac{1}{2} m_\rho^2\vec{\rho}_\mu\vec{\rho}^\mu, \tag{10}
\end{aligned}$$

where a scalar-isovector meson (δ) is also introduced due to some parameterization. The coupling constants of σ and ω mesons are usually expressed as a fraction function of the total vector density, $\rho_B = \sum_B \rho_B^v$. In most of DDRMF parametrizations, such as DD2 [111], DD-ME1 [112], DD-ME2 [113], DDME-X [114], PKDD [115], TW99 [116], and DDV, DDVT, DDVTD [117], they are assumed as,

$$\Gamma_{iN}(\rho_B) = \Gamma_{iN}(\rho_{B0})f_i(x) \tag{11}$$

with

$$f_i(x) = a_i \frac{1 + b_i(x + d_i)^2}{1 + c_i(x + d_i)^2}, \quad x = \rho_B/\rho_{B0}, \tag{12}$$

for $i = \sigma, \omega$. ρ_{B0} is the saturation density of symmetric nuclear matter. Five constraints on the coupling constants $f_i(1) = 1$, $f_i''(0) = 0$, $f_\sigma''(1) = f_\omega''(1)$ can reduce the numbers of independent parameters to three in Eq. (12). The first two constraints lead to

$$a_i = \frac{1 + c_i(1 + d_i)^2}{1 + b_i(1 + d_i)^2}, \quad 3c_id_i^2 = 1. \tag{13}$$

For the isovector mesons ρ and δ , their density-dependent coupling constants are assumed to be,

$$\Gamma_{iN}(\rho_B) = \Gamma_{iN}(\rho_{B0})\exp[-a_i(x - 1)]. \tag{14}$$

While in other parametrizations, such as DD-LZ1 [118], the coefficient in front of fraction function, Γ_i is fixed at $\rho_B = 0$ for $i = \sigma, \omega$:

$$\Gamma_{iN}(\rho_B) = \Gamma_{iN}(0)f_i(x). \quad (15)$$

There are only four constraint conditions as $f_i(0) = 1$ and $f_i''(0) = 0$ for σ and ω coupling constants in DD-LZ1 set. The constraint $f_\sigma''(1) = f_\omega''(1)$ in previous parameter sets was removed in DD-LZ1 parametrization. For ρ meson, its coupling constant is also changed accordingly as

$$\Gamma_{\rho N}(\rho_B) = \Gamma_{\rho N}(0)\exp(-a_\rho x). \quad (16)$$

Within the mean-field approximation, the meson fields are treated as the classical fields, $\langle \sigma \rangle = \sigma$, $\langle \sigma^* \rangle = \sigma^*$, $\langle \omega_\mu \rangle = \omega$, $\langle \phi_\mu \rangle = \phi$, $\langle \vec{\rho}_\mu \rangle = \rho$, $\langle \delta \rangle = \delta$. Together with the Euler-Lagrange equations, the equations of motion for baryons and mesons are given by :

$$\begin{aligned} & \left[i\gamma^\mu \partial_\mu - \gamma^0 \left(\Gamma_{\omega B}(\rho_B)\omega + \Gamma_{\phi B}(\rho_B)\phi \right. \right. \\ & \left. \left. + \frac{\Gamma_{\rho B}(\rho_B)}{2}\rho\tau_3 + \Sigma_R(\rho_B) \right) - M_B^* \right] \psi_B = 0. \\ m_\sigma^2 \sigma &= \sum_B \Gamma_{\sigma B}(\rho_B)\rho_B^s, \\ m_{\sigma^*}^2 \sigma^* &= \sum_B \Gamma_{\sigma^* B}(\rho_B)\rho_B^s, \\ m_\omega^2 \omega &= \sum_B \Gamma_{\omega B}(\rho_B)\rho_B^v, \\ m_\phi^2 \phi &= \sum_B \Gamma_{\phi B}(\rho_B)\rho_B^v, \\ m_\rho^2 \rho &= \sum_B \frac{\Gamma_{\rho B}(\rho_B)}{2}\rho_B^{v3}, \\ m_\delta^2 \delta &= \sum_B \Gamma_{\delta B}(\rho_B)\rho_B^{s3}. \end{aligned} \quad (17)$$

Comparing to the NLRMF model, an additional term about the rearrangement contribution, Σ_R will be introduced into the vector potential in Eq. (17) due to the vector density-

dependence of coupling constants,

$$\begin{aligned}\Sigma_R(\rho_B) = & -\frac{\partial\Gamma_{\sigma B}(\rho_B)}{\partial\rho_B}\sigma\rho_B^s - \frac{\partial\Gamma_{\sigma^* B}(\rho_B)}{\partial\rho_B}\sigma^*\rho_B^s \\ & - \frac{\partial\Gamma_{\delta B}(\rho_B)}{\partial\rho_B}\delta\rho_B^{s3} + \frac{1}{2}\frac{\partial\Gamma_{\rho B}(\rho_B)}{\partial\rho_B}\rho\rho_B^{v3} \\ & + \left[\frac{\partial\Gamma_{\omega B}(\rho_B)}{\partial\rho_B}\omega + \frac{\partial\Gamma_{\phi B}(\rho_B)}{\partial\rho_B}\phi \right] \rho_B^v,\end{aligned}\quad (18)$$

where the scalar, vector densities, and their isospin components take the same forms as shown in Eq. (4). The effective masses of baryons in Eq. (17) are dependent on the scalar mesons σ , σ^* and δ ,

$$M_B^* = M_B - \Gamma_{\sigma B}(\rho_B)\sigma - \Gamma_{\sigma^* B}(\rho_B)\sigma^* - \Gamma_{\delta B}(\rho_B)\delta\tau_3 \quad (19)$$

and the corresponding effective energies of baryons take the same form as Eq. (6).

The energy density, \mathcal{E} and pressure, P of nuclear matter in DDRMF model are obtained respectively as

$$\begin{aligned}\mathcal{E}_{\text{DD}} = & \frac{1}{2}m_\sigma^2\sigma^2 + \frac{1}{2}m_{\sigma^*}^2\sigma^{*2} - \frac{1}{2}m_\omega^2\omega^2 - \frac{1}{2}m_\phi^2\phi^2 \\ & - \frac{1}{2}m_\rho^2\rho^2 + \frac{1}{2}m_\delta^2\delta^2 + \Gamma_{\omega B}(\rho_B)\omega\rho_B \\ & + \Gamma_{\phi B}(\rho_B)\phi\rho_B + \frac{\Gamma_\rho(\rho_B)}{2}\rho\rho_3 + \mathcal{E}_{\text{kin}}^B, \\ P_{\text{DD}} = & \rho_B\Sigma_R(\rho_B) - \frac{1}{2}m_\sigma^2\sigma^2 - \frac{1}{2}m_{\sigma^*}^2\sigma^{*2} \\ & + \frac{1}{2}m_\omega^2\omega^2 + \frac{1}{2}m_\phi^2\phi^2 + \frac{1}{2}m_\rho^2\rho^2 \\ & - \frac{1}{2}m_\delta^2\delta^2 + P_{\text{kin}}^B,\end{aligned}\quad (20)$$

where, the contributions from kinetic energy are

$$\begin{aligned}\mathcal{E}_{\text{kin}}^B = & \frac{\gamma}{2\pi^2} \int_0^{k_{FB}} k^2 \sqrt{k^2 + M_B^{*2}} dk \\ = & \frac{\gamma}{16\pi^2} \left[k_{FB} E_{FB}^* (2k_{FB}^2 + M_B^{*2}) \right. \\ & \left. + M_B^{*4} \ln \frac{M_B^*}{k_{FB} + E_{FB}^*} \right],\end{aligned}\quad (21)$$

$$\begin{aligned}P_{\text{kin}}^B = & \frac{\gamma}{6\pi^2} \int_0^{k_{FB}} \frac{k^4 dk}{\sqrt{k^2 + M_B^{*2}}} \\ = & \frac{\gamma}{48\pi^2} \left[k_{FB} (2k_{FB}^2 - 3M_B^{*2}) E_{FB}^* \right. \\ & \left. + 3M_B^{*4} \ln \frac{k_{FB} + E_{FB}^*}{M_B^*} \right].\end{aligned}\quad (22)$$

$\gamma = 2$ is the spin degeneracy factor.

The chemical potentials of baryons and leptons are

$$\begin{aligned}\mu_B &= \sqrt{k_{FB}^2 + M_B^{*2}} + [\Gamma_{\omega B}(\rho_B)\omega + \Gamma_{\phi B}(\rho_B)\phi \\ &\quad + \frac{\Gamma_{\rho B}(\rho_B)}{2}\rho\tau_3 + \Sigma_R(\rho_B)], \\ \mu_l &= \sqrt{k_{Fl}^2 + m_l^2}.\end{aligned}\tag{23}$$

C. The formulas about neutron star

In the uniform hyperonic star matter, the compositions of baryons and leptons are determined by the requirements of charge neutrality and β -equilibrium conditions. All baryon octets (n , p , Λ , Σ^- , Σ^0 , Σ^+ , Ξ^- , Ξ^0) and leptons (e , μ) will be included in this work. The β -equilibrium conditions can be expressed by [61, 75]

$$\begin{aligned}\mu_p &= \mu_{\Sigma^+} = \mu_n - \mu_e, \\ \mu_\Lambda &= \mu_{\Sigma^0} = \mu_{\Xi^0} = \mu_n, \\ \mu_{\Sigma^-} &= \mu_{\Xi^-} = \mu_n + \mu_e, \\ \mu_\mu &= \mu_e.\end{aligned}\tag{24}$$

The charge neutrality condition has the following form,

$$\rho_p^v + \rho_{\Sigma^+}^v = \rho_e^v + \rho_\mu^v + \rho_{\Sigma^-}^v + \rho_{\Xi^-}^v.\tag{25}$$

The total energy density and pressure of neutron star matter will be obtained as a function of baryon density within the constraints of Eqs. (24) and (25). The Tolman-Oppenheimer-Volkoff (TOV) equation describes a spherically symmetric star in the gravitational equilibrium from general relativity [119, 120],

$$\begin{aligned}\frac{dP}{dr} &= -\frac{GM(r)\mathcal{E}(r)}{r^2} \frac{\left[1 + \frac{P(r)}{\mathcal{E}(r)}\right] \left[1 + \frac{4\pi r^3 P(r)}{M(r)}\right]}{1 - \frac{2GM(r)}{r}}, \\ \frac{dM(r)}{dr} &= 4\pi r^2 \mathcal{E}(r),\end{aligned}\tag{26}$$

where P and M are the pressure and mass of a neutron star at the position r . Furthermore, the tidal deformability becomes a typical property of a neutron star after the observation of the gravitational wave from a binary neutron-star (BNS) merger, which characterizes the

deformation of a compact object in an external gravity field generated by another star. The tidal deformability of a neutron star is reduced as a dimensionless form [121, 122],

$$\Lambda = \frac{2}{3}k_2C^{-5}. \quad (27)$$

where $C = GM/R$ is the compactness parameter. The second order Love number k_2 is given by

$$\begin{aligned} k_2 = & \frac{8C^5}{5}(1-2C)^2 [2 + 2C(\mathcal{Y}_R - 1) - \mathcal{Y}_R] \\ & \left\{ 2C [6 - 3\mathcal{Y}_R + 3C(5\mathcal{Y}_R - 8)] \right. \\ & + 4C^3 [13 - 11\mathcal{Y}_R + C(3\mathcal{Y}_R - 2) + 2C^2(1 + \mathcal{Y}_R)] \\ & \left. + 3(1-2C)^2 [2 - \mathcal{Y}_R + 2C(\mathcal{Y}_R - 1)\ln(1-2C)] \right\}^{-1}. \end{aligned} \quad (28)$$

Here, $\mathcal{Y}_R = y(R)$. $y(r)$ satisfies the following first-order differential equation,

$$r \frac{dy(r)}{dr} + y^2(r) + y(r)F(r) + r^2Q(r) = 0, \quad (29)$$

where $F(r)$ and $Q(r)$ are functions related to the pressure and energy density

$$\begin{aligned} F(r) &= \left[1 - \frac{2M(r)}{r} \right]^{-1} \{ 1 - 4\pi r^2 [\mathcal{E}(r) - P(r)] \}, \\ r^2Q(r) &= \left\{ 4\pi r^2 \left[5\mathcal{E}(r) + 9P(r) + \frac{\mathcal{E}(r) + P(r)}{\frac{\partial P}{\partial \mathcal{E}}(r)} \right] - 6 \right\} \\ &\quad \times \left[1 - \frac{2M(r)}{r} \right]^{-1} - \left[\frac{2M(r)}{r} + 2 \times 4\pi r^2 P(r) \right]^2 \\ &\quad \times \left[1 - \frac{2M(r)}{r} \right]^{-2}. \end{aligned} \quad (30)$$

The second Love number corresponds to the initial condition $y(0) = 2$. It is also related to the speed of sound in compact matter, c_s ,

$$c_s^2 = \frac{\partial P(\varepsilon)}{\partial \mathcal{E}}. \quad (31)$$

III. RESULTS AND DISCUSSIONS

A. The RMF Parametrizations

In the present work, four popular parameter sets, TM1 [101], NL3 [123], IUFSU [124], and BigApple [125] in the NLRMF model are used to describe the uniform matter, which

was generated by fitting the ground state properties of several stable nuclei. The nonlinear term of the vector meson was considered in the TM1 set to reproduce the nucleon vector potential from the RBHF model. The NL3 set can generate a large maximum mass of a neutron star, while its radius is large [58]. The ω - ρ meson coupling term was included in the IUFSU set. The BigApple set can lead to a large maximum mass of a neutron star with a small radius due to the smaller slope of the symmetry energy [125]. The masses of nucleons and mesons, and the coupling constants between nucleon and mesons in NLRMF models, TM1 [101], IUFSU [124], BigApple [125], NL3 [123] are tabulated in Table I.

TABLE I. Masses of nucleons and mesons, meson coupling constants in various NLRMF models

	NL3 [123]	BigApple [125]	TM1 [101]	IUFSU [124]
m_n [MeV]	939.000	939.000	938.000	939.000
m_p [MeV]	939.000	939.000	938.000	939.000
m_σ [MeV]	508.194	492.730	511.198	491.500
m_ω [MeV]	782.501	782.500	783.000	782.500
m_ρ [MeV]	763.000	763.000	770.000	763.000
g_σ	10.217	9.6699	10.0289	9.9713
g_ω	12.868	12.316	12.6139	13.0321
g_ρ	8.948	14.1618	9.2644	13.5899
$g_2(\text{fm}^{-1})$	10.431	11.9214	7.2325	8.4929
g_3	-28.885	-31.6796	0.6183	0.4877
c_3	0.000	2.6843	71.3075	144.2195
Λ_V	0.000	0.047471	0.000	0.046

For the DDRMF models, the parametrizations, DD2 [111], DD-ME1 [112], DD-ME2 [113], DDME-X [113], PKDD [115], TW99 [116], DDV, DDVT, DDVTD [117], and DD-LZ1 [118] are listed in Table II. TW99, DD2, DD-ME1, DD-ME2, and PKDD parameter sets were obtained by reproducing the ground-state properties of different nuclei before 2005. In recent years, the DDME-X, DD-LZ1, DDV, DDVT, and DDVTD sets were brought out with various considerations. In DDVT and DDVTD sets, the tensor coupling between the vector meson and nucleon was included. The scalar-isovector meson, δ was taken into account in DDVTD. The coefficients of meson coupling constants, Γ_i in DD-LZ1 are the values at zero density, while other parameter sets are dependent on the values at nuclear saturation densities.

The saturation properties of symmetric nuclear matter calculated with different RMF

TABLE II. Masses of nucleons and mesons, meson coupling constants, and the nuclear saturation densities in various DDRMF models.

	DD-LZ1 [118]		DD-MEX [114]	DD-ME2 [113]	DD-ME1 [112]	DD2 [111]	PKDD [115]	TW99 [116]	DDV [117]	DDVT [117]	DDVTD [117]
m_n [MeV]	938.900000	m_n	939.0000	939.0000	939.0000	939.56536	939.5731	939.0000	939.565413	939.565413	939.565413
m_p [MeV]	938.900000	m_p	939.0000	939.0000	939.0000	938.27203	938.2796	939.0000	938.272081	938.272081	938.272081
m_σ [MeV]	538.619216	m_σ	547.3327	550.1238	549.5255	546.212459	555.5112	550.0000	537.600098	502.598602	502.619843
m_ω [MeV]	783.0000	m_ω	783.0000	783.0000	783.0000	783.0000	783.0000	783.0000	783.0000	783.0000	783.0000
m_ρ [MeV]	769.0000	m_ρ	763.0000	763.0000	763.0000	763.0000	763.0000	763.0000	763.0000	763.0000	763.0000
m_δ [MeV]	—	m_δ	—	—	—	—	—	—	—	—	980.0000
$\Gamma_\sigma(0)$	12.001429	$\Gamma_\sigma(\rho_{B0})$	10.7067	10.5396	10.4434	10.686681	10.7385	10.72854	10.136960	8.382863	8.379269
$\Gamma_\omega(0)$	14.292525	$\Gamma_\omega(\rho_{B0})$	13.3388	13.0189	12.8939	13.342362	13.1476	13.29015	12.770450	10.987106	10.980433
$\Gamma_\rho(0)$	15.150934	$\Gamma_\rho(\rho_{B0})$	7.2380	7.3672	7.6106	7.25388	8.5996	7.32196	7.84833	7.697112	8.06038
$\Gamma_\delta(0)$	—	$\Gamma_\delta(\rho_{B0})$	—	—	—	—	—	—	—	—	0.8487420
ρ_{B0} [fm $^{-3}$]	0.1581	ρ_{B0}	0.1520	0.1520	0.1520	0.1490	0.1496	0.1530	0.1511	0.1536	0.1536
a_σ	1.062748	a_σ	1.3970	1.3881	1.3854	1.357630	1.327423	1.365469	1.20993	1.20397	1.19643
b_σ	1.763627	b_σ	1.3350	1.0943	0.9781	0.634442	0.435126	0.226061	0.21286844	0.19210314	0.19171263
c_σ	2.308928	c_σ	2.0671	1.7057	1.5342	1.005358	0.691666	0.409704	0.30798197	0.27773566	0.27376859
d_σ	0.379957	d_σ	0.4016	0.4421	0.4661	0.575810	0.694210	0.901995	1.04034342	1.09552817	1.10343705
a_ω	1.059181	a_ω	1.3936	1.3892	1.3879	1.369718	1.342170	1.402488	1.23746	1.16084	1.16693
b_ω	0.418273	b_ω	1.0191	0.9240	0.8525	0.496475	0.371167	0.172577	0.03911422	0.04459850	0.02640016
c_ω	0.538663	c_ω	1.6060	1.4620	1.3566	0.817753	0.611397	0.344293	0.07239939	0.06721759	0.04233010
d_ω	0.786649	d_ω	0.4556	0.4775	0.4957	0.638452	0.738376	0.983955	2.14571442	2.22688558	2.80617483
a_ρ	0.776095	a_ρ	0.6202	0.5647	0.5008	0.518903	0.183305	0.5150	0.35265899	0.54870200	0.55795902
a_δ	—	a_δ	—	—	—	—	—	—	—	—	0.55795902

effective interactions are listed in Table III, i.e. the saturation density, ρ_0 , the binding energy per nucleon, E/A , incompressibility, K_0 , symmetry energy, E_{sym} , the slope of symmetry energy, L , and the effective neutron and proton masses, M_n^* and M_p^* . The saturation densities of nuclear matter are in the region of $0.145 - 0.158 \text{ fm}^{-3}$. The binding energies per nucleon at saturation density are around -16.5 MeV . The incompressibilities of nuclear matter are $230 \sim 280 \text{ MeV}$. The symmetry energies are $31 \sim 37 \text{ MeV}$. The slopes of the symmetry energy from these RMF interactions have large uncertainties, from $40 - 120 \text{ MeV}$, since there are still not too many experimental constraints about the neutron skin [126–131]. The effective mass differences between neutron and proton in this table are caused by the differences of their free masses.

For the hyperonic star matter with strangeness degree of freedom, the hyperon masses are chosen as $m_\Lambda = 1115.68 \text{ MeV}$, $m_{\Sigma^+} = 1189.37 \text{ MeV}$, $m_{\Sigma^0} = 1192.64 \text{ MeV}$, $m_{\Sigma^-} = 1197.45 \text{ MeV}$, $m_{\Xi^0} = 1314.86 \text{ MeV}$, and $m_{\Xi^-} = 1321.71 \text{ MeV}$ [132], while the masses of strange mesons, ϕ and σ^* are taken as $m_\phi = 1020 \text{ MeV}$ and $m_\phi = 980 \text{ MeV}$. We adopt the values from

TABLE III. Nuclear matter properties at saturation density generated by NLRMF and DDRMF parameterizations.

	$\rho_{B0}[\text{fm}^{-3}]$	$E/A[\text{MeV}]$	$K_0[\text{MeV}]$	$E_{\text{sym}}[\text{MeV}]$	$L_0[\text{MeV}]$	M_n^*/M	M_p^*/M
NL3	0.1480	-16.2403	269.9605	37.3449	118.3225	0.5956	0.5956
BigApple	0.1545	-16.3436	226.2862	31.3039	39.7407	0.6103	0.6103
TM1	0.1450	-16.2631	279.5858	36.8357	110.6082	0.6348	0.6348
IUFSU	0.1545	-16.3973	230.7491	31.2851	47.1651	0.6095	0.6095
DD-LZ1	0.1581	-16.0598	231.1030	31.3806	42.4660	0.5581	0.5581
DD-MEX	0.1519	-16.0973	267.3819	32.2238	46.6998	0.5554	0.5554
DD-ME2	0.1520	-16.1418	251.3062	32.3094	51.2653	0.5718	0.5718
DD-ME1	0.1522	-16.2328	245.6657	33.0899	55.4634	0.5776	0.5776
DD2	0.1491	-16.6679	242.8509	31.6504	54.9529	0.5627	0.5614
PKDD	0.1495	-16.9145	261.7912	36.7605	90.1204	0.5713	0.5699
TW99	0.1530	-16.2472	240.2022	32.7651	55.3095	0.5549	0.5549
DDV	0.1511	-16.9279	239.9522	33.5969	69.6813	0.5869	0.5852
DDVT	0.1536	-16.9155	239.9989	31.5585	42.3414	0.6670	0.6657
DDVTD	0.1536	-16.9165	239.9137	31.8168	42.5829	0.6673	0.6660

the SU(6) symmetry for the coupling constants between hyperons and vector mesons [133],

$$\begin{aligned}
\Gamma_{\omega\Lambda} &= \Gamma_{\omega\Sigma} = 2\Gamma_{\omega\Xi} = \frac{2}{3}\Gamma_{\omega N}, \\
2\Gamma_{\phi\Sigma} &= \Gamma_{\phi\Xi} = -\frac{2\sqrt{2}}{3}\Gamma_{\omega N}, \quad \Gamma_{\phi N} = 0, \\
\Gamma_{\rho\Lambda} &= 0, \quad \Gamma_{\rho\Sigma} = 2\Gamma_{\rho\Xi} = 2\Gamma_{\rho N}, \\
\Gamma_{\delta\Lambda} &= 0, \quad \Gamma_{\delta\Sigma} = 2\Gamma_{\delta\Xi} = 2\Gamma_{\delta N}.
\end{aligned} \tag{32}$$

The coupling constants of hyperon and scalar mesons are constrained by the hyperon-nucleon potentials in symmetric nuclear matter, U_Y^N , which are defined by

$$U_Y^N(\rho_{B0}) = -R_{\sigma Y}\Gamma_{\sigma N}(\rho_{B0})\sigma_0 + R_{\omega Y}\Gamma_{\omega N}(\rho_{B0})\omega_0, \tag{33}$$

where $\Gamma_{\sigma N}(\rho_{B0})$, $\Gamma_{\omega N}(\rho_{B0})$, σ_0 , ω_0 are the values of coupling strengths and σ , ω meson fields at the saturation density. $R_{\sigma Y}$ and $R_{\omega Y}$ are defined as $R_{\sigma Y} = \Gamma_{\sigma Y}/\Gamma_{\sigma N}$ and $R_{\omega Y} = \Gamma_{\omega Y}/\Gamma_{\omega N}$. We choose the hyperon-nucleon potentials of Λ , Σ and Ξ as $U_\Lambda^N = -30$ MeV, $U_\Sigma^N = +30$ MeV and $U_\Xi^N = -14$ MeV, respectively from the recent hypernuclei experimental observables [72, 80, 134].

The coupling constants between Λ and σ^* is generated by the value of the $\Lambda\Lambda$ potential in pure Λ matter, U_Λ^Λ at nuclear saturation density, which is given as

$$\begin{aligned}
U_\Lambda^\Lambda(\rho_{B0}) = & -R_{\sigma\Lambda}\Gamma_{\sigma N}(\rho_{B0})\sigma_0 - R_{\sigma^*\Lambda}\Gamma_{\sigma N}(\rho_{B0})\sigma_0^* \\
& + R_{\omega Y}\Gamma_{\omega N}(\rho_{B0})\omega_0 + R_{\phi\Lambda}\Gamma_{\omega N}(\rho_{B0})\phi_0,
\end{aligned}
\tag{34}$$

We similarly define that $R_{\sigma^*\Lambda} = \Gamma_{\sigma^*\Lambda}/\Gamma_{\sigma N}$ and $R_{\phi\Lambda} = \Gamma_{\phi\Lambda}/\Gamma_{\omega N}$. $R_{\sigma^*\Lambda}$ is obtained from the $\Lambda - \Lambda$ potential as $U_\Lambda^\Lambda(\rho_{B0}) = -10$ MeV, which was extracted from the Λ bonding energies of double- Λ hypernuclei. $R_{\phi\Lambda} = -\sqrt{2}/2$ is corresponding to the SU(6) symmetry broken case [80]. Here, the coupling between the Σ , Ξ hyperons and σ^* mesons are set as $R_{\sigma^*\Xi} = 0$, $R_{\sigma^*\Sigma} = 0$, since the information about their interaction is absent until now. The values of $R_{\sigma Y}$ and $R_{\sigma^*\Lambda}$ with above constraints in different RMF effective interactions are shown in Table IV.

TABLE IV. The Coupling constants between hyperons and σ meson, $g_{\sigma Y}$ and Λ - σ^* , $g_{\sigma^*\Lambda}$ in different RMF effective interactions.

	$R_{\sigma\Lambda}$	$R_{\sigma\Sigma}$	$R_{\sigma\Xi}$	$R_{\sigma^*\Lambda}$
NL3	0.618896	0.460889	0.306814	0.84695
BigApple	0.616322	0.452837	0.305436	0.86313
TM1	0.621052	0.445880	0.307606	0.83710
IUFSU	0.616218	0.453006	0.305389	0.88802
DD-LZ1	0.610426	0.465708	0.302801	0.87595
DD-MEX	0.612811	0.469159	0.304011	0.86230
DD-ME2	0.609941	0.460706	0.302483	0.85758
DD-ME1	0.608602	0.457163	0.301777	0.85828
DD2	0.612743	0.466628	0.303937	0.86420
PKDD	0.610412	0.461807	0.302729	0.84965
TW99	0.612049	0.468796	0.303632	0.85818
DDV	0.607355	0.452777	0.301101	0.87979
DDVT	0.591179	0.399269	0.292391	0.92256
DDVTD	0.591108	0.399023	0.292352	0.92246

B. Neutron Star and Hyperonic Star

With the conditions of β equilibrium and charge neutrality, the equations of state (EoSs) of neutron star matter including the neutron, proton, and leptons, i.e. the $P - \epsilon$ function in the NLRMF and DDRMF models is obtained in the panel (a) and panel (b) of Fig. (1), which shows the pressures of neutron star matter as a function of energy density. For the inner crust part of a neutron star, the EoS of the non-uniform matter generated by TM1 parametrization with self-consistent Thomas-Fermi approximation is adopted [38]. In the core region of a neutron star, the EoSs of the uniform matter are calculated with various NLRMF and DDRMF parameter sets. Furthermore, the joint constraints on the EoS extracted from the GW170817 and GW190814 are shown as a shaded band [21], which was obtained from the gravitational wave signal by Bayesian method with the spectral EoS parametrizations [18]. The pressures from TM1 and NL3 sets around saturation density are larger than those from IUFSU and BigApple sets since their incompressibilities K_0 are about 270 – 280 MeV. At the high-density region, the EoSs from NL3 and BigApple become stiffer since g_3 in these two sets are negative, which will produce smaller scalar fields and provide less attractive contributions to the EoSs. In DDRMF parameter sets, the EoSs have similar density-dependent behaviors. The DDV, DDVT, DDVTD, and TW99 sets generate the softer EoSs compared to other sets.

After considering more conditions of beta equilibrium and charge neutrality about the hyperons, the EoSs of hyperonic star matter from the NLRMF and DDRMF models, where the coupling strengths between the mesons and hyperons are described as before, can be obtained in panel (c) and panel (d) of Fig. (1). They almost become softer from $\epsilon \sim 300$ MeV/fm³ compared to the neutron star matter, due to the appearances of hyperons. In high-density region, all of them are below the joint constraints on the EoS from GW170817 and GW190814 events.

Similarly, in panel (a) and panel (b) of Fig. (2), the pressures as functions of baryon density in neutron star matter from NLRMF and DDRMF models are given. Furthermore, the speeds of sound in neutron star matter, c_s with the unit of light speed are plotted in the insert. Since the NLRMF and DDRMF models are constructed based on the relativistic theory, the speeds of the sound from the RMF framework should be less than 1 due to the causality. The NL3 set brings out the largest speed of the sound, while the c_s^2/c^2 from TM1

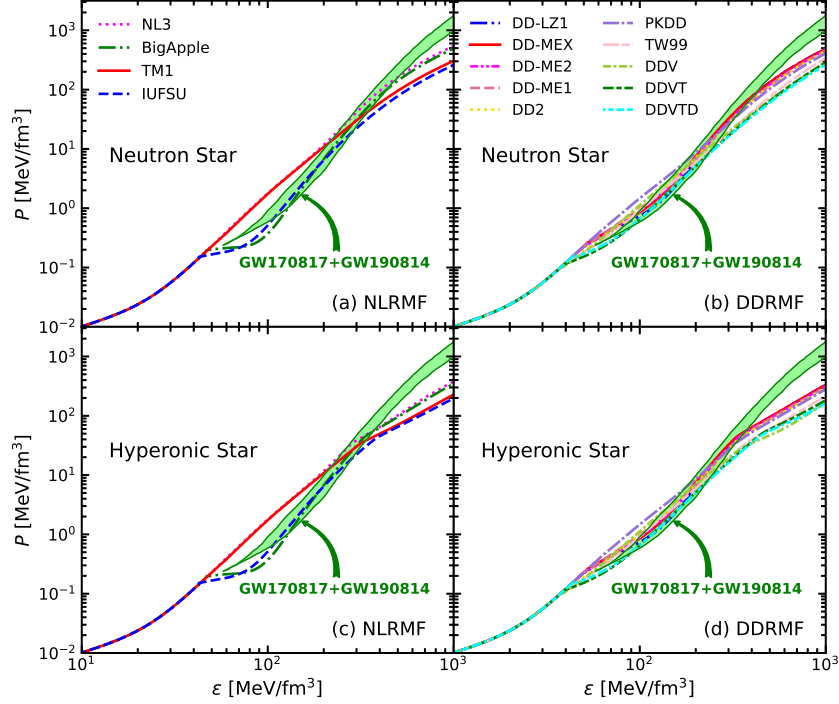


FIG. 1. The pressure P versus energy density ε of neutron star matter and hyperonic star matter from NLRMF and DDRMF models. The joint constraints on EoS extracted from the GW170817 and GW190814 are shown as a shaded green band. Panels (a) and panel (b) for the neutrons star matter from the NLRMF and DDRMF models, respectively. Panels (c) and panel (d) for the hyperonic star matter from the NLRMF and DDRMF models, respectively.

and IUFSU sets at high density approach 0.4. It is noteworthy that c_s^2/c^2 is 1/3 from the conformal limit of quark matter [54, 56].

The pressures as functions of density in hyperonic star matter from NLRMF and DDRMF models are given in panel (c) and panel (d), respectively. The onset densities of the first hyperon are marked by the full discretized symbols, which are around $0.28 - 0.45 \text{ fm}^{-3}$. The speed of sound of hyperonic star matter is not smooth as a function density anymore. The appearance of hyperon can sharply reduce the magnitude of the speed of sound, especially at first onset density. For the hard EoS, the c_s^2 becomes 0.6 in hyperonic star matter from 0.8 in neutron star matter at high-density region.

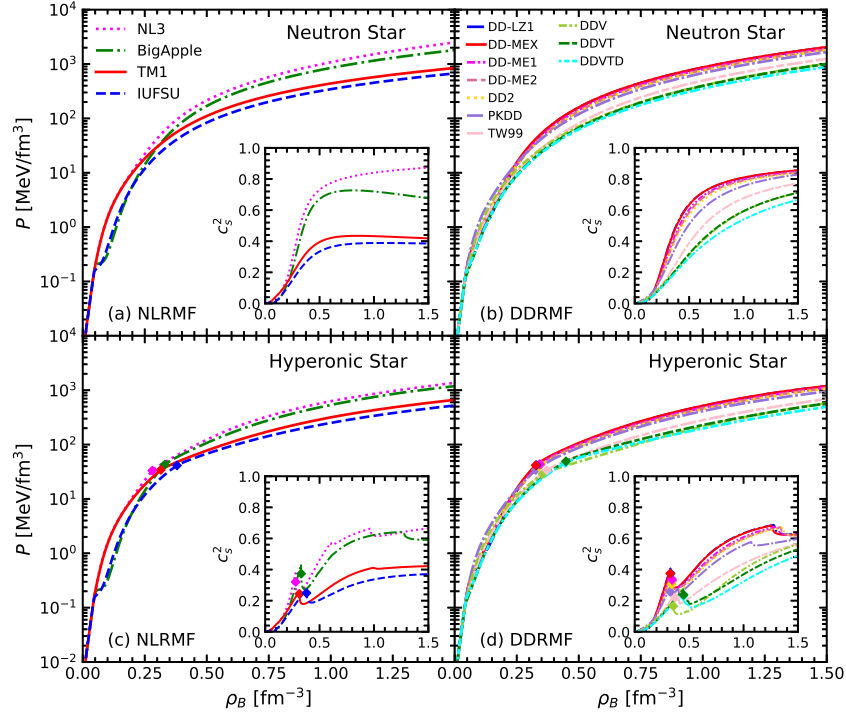


FIG. 2. EoSs of neutron star and hyperonic star matter with different NLRMF and DDRMF models. The corresponding speeds of sound in units of the speed of light shown in the insert. Panels (a) and panel (b) for the neutrons star matter from the NLRMF and DDRMF models, respectively. Panels (c) and panel (d) for the hyperonic star matter from the NLRMF and DDRMF models, respectively.

The onset densities of Λ , Σ , and Ξ hyperons in various NLRMF and DDRMF models are listed in Table.(V). In general, the Λ hyperon firstly arises around $2 - 3\rho_0$ due to its small mass and large attractive ΛN potential. The most probable baryon of the second onset is the Σ^- hyperon for $\rho_B < 4\rho_0$, whose mass is very close to that of the Λ hyperon. In a few parameter sets, such as NL3, PKDD, DDVT, and DDVTD, the second appearing hyperon is the Ξ^- hyperon, which can bind with the nucleons to form the Ξ^- hypernuclei. With the density increasing, the Ξ^- hyperon usually emerges above $4\rho_0$ and Ξ^0 appears above $7\rho_0$.

The corresponding particle fractions of baryons as a function of baryon number density with different NLRMF and DDRMF parameter sets are shown in Fig. (3) and Fig. (4),

TABLE V. Hyperon thresholds calculated with different RMF effective interactions for hyperonic matter. The unit of the density is fm^{-3} .

	1 st (ρ_{th})	2 nd (ρ_{th})	3 rd (ρ_{th})	4 th (ρ_{th})
NL3	Λ (0.2804)	Ξ^- (0.6078)	Ξ^0 (0.9723)	Σ^- (1.3545)
BigApple	Λ (0.3310)	Σ^- (0.4895)	Ξ^- (0.6191)	Ξ^0 (1.2758)
TM1	Λ (0.3146)	Σ^- (0.9995)	Ξ^- (1.0228)	
IUFSU	Λ (0.3800)	Σ^- (0.5645)		
DD-LZ1	Λ (0.3294)	Σ^- (0.4034)	Ξ^- (0.6106)	Ξ^0 (1.2935)
DD-MEX	Λ (0.3264)	Σ^- (0.3871)	Ξ^- (0.5967)	Ξ^0 (1.2699)
DD-ME2	Λ (0.3402)	Σ^- (0.4244)	Ξ^- (0.4895)	Ξ^0 (1.3237)
DD-ME1	Λ (0.3466)	Σ^- (0.4424)	Ξ^- (0.4740)	Ξ^0 (1.3545)
DD2	Λ (0.3387)	Σ^- (0.4147)	Ξ^- (0.5699)	Ξ^0 (1.3733)
PKDD	Λ (0.3264)	Ξ^- (0.4016)	Σ^- (0.5126)	Ξ^0 (1.0759)
TW99	Λ (0.3696)	Σ^- (0.4167)	Ξ^- (0.7109)	Ξ^0 (1.7052)
DDV	Λ (0.3547)	Σ^- (0.4850)	Ξ^- (0.7723)	
DDVT	Λ (0.4465)	Ξ^- (0.4941)	Σ^- (0.6220)	
DDVTD	Λ (0.4465)	Ξ^- (0.4963)	Σ^- (0.6163)	

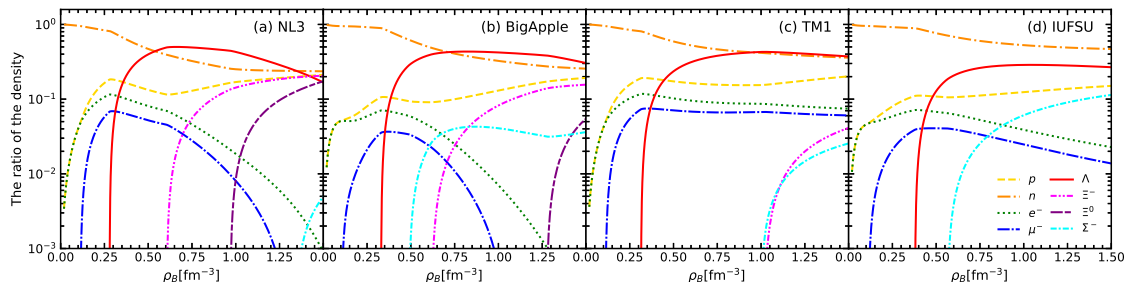


FIG. 3. Particle fractions of baryons as a function of baryon number density with different NLRMF parameter sets.

respectively. At a low-density region, the hyperonic matter is almost consisting of neutrons. The proton and electron fractions rapidly increase with density. When the chemical potential of the electron is larger than the free muon mass, the muon will arise. Above $2\rho_0$, the various hyperons appear in the hyperonic matter when they satisfy the chemical equilibrium conditions. At the high-density region, the fractions of various particles are strongly dependent on the NN and NY interactions. However, at all events, the fractions of Λ hyperon will approach that of neutrons. In some cases, it can exceed those of neutrons.

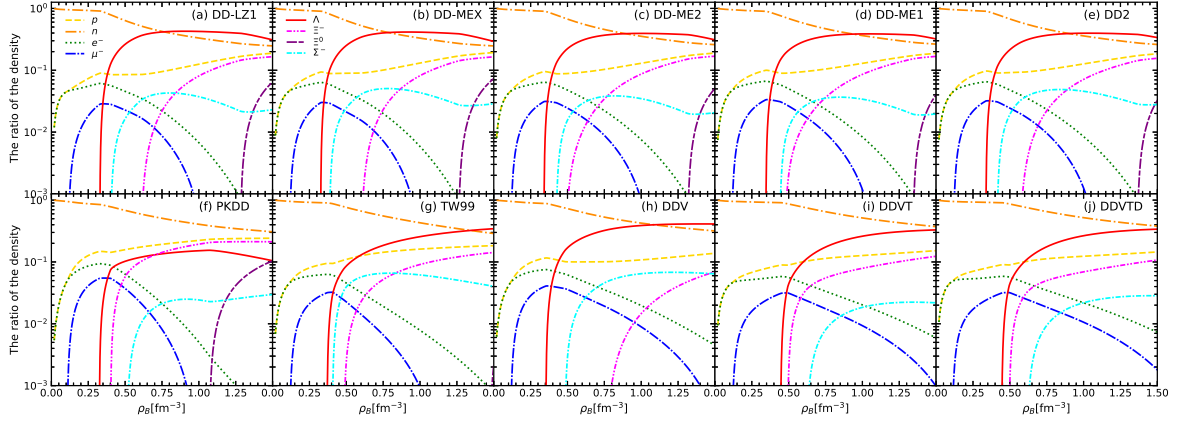


FIG. 4. Particle fractions of baryons as a function of baryon number density with different DDRMF parameter sets.

After solving the TOV equation, the mass-radius relation of a static neutron star is obtained, where the EoSs of neutron star matter in the previous part are used. In Fig. (5), the mass-radius ($M - R$) relations from NLRMF sets and DDRMF sets are shown in panel (a) and panel (b), respectively. The constraints from the observables of massive neutron stars, PSR J1614-2230 and PSR J034+0432 are also shown as the shaded bands. In 2019, the Neutron star Interior Composition Explorer (NICER) collaboration reported an accurate measurement of mass and radius of PSR J0030+0451, simultaneously. It may be a mass of $1.44^{+0.15}_{-0.14} M_{\odot}$ with a radius of $13.02^{+1.24}_{-1.06}$ km [135] and a mass of $1.34^{+0.15}_{-0.16} M_{\odot}$ with a radius of $12.71^{+1.14}_{-1.19}$ km [136] by two independent analysis groups. Recently, the radius of the pulsar PSR J0740+6620 with mass was reported by two independent groups based on NICER and X-ray Multi-Mirror (XMM-Newton) observations. The inferred radius of this massive NS is constrained to $12.39^{+1.30}_{-0.98}$ km for the mass $2.072^{+0.0067}_{-0.066} M_{\odot}$ by Riley *et al.* [137] and $13.7^{+2.6}_{-1.5}$ km for the mass $2.08 \pm 0.07 M_{\odot}$ by Miller *et al.* at 68% credible level [16]. These constraints from NICER analyzed by Riley *et al.* are plotted in Fig. (5). Meanwhile, the radius at $1.4 M_{\odot}$ extracted from GW170817 is also shown [18].

Among all parameter set used, NL3 predicts the heaviest neutron star mass ($2.77 M_{\odot}$) due to its hard EoS, while the corresponding radius at $1.4 M_{\odot}$ does not satisfy the measurements from GW170817 and NICER. It can be found that the radii at $1.4 M_{\odot}$ from NL3 and TM1 sets are much larger than those from other RMF sets. This is caused by their large slope

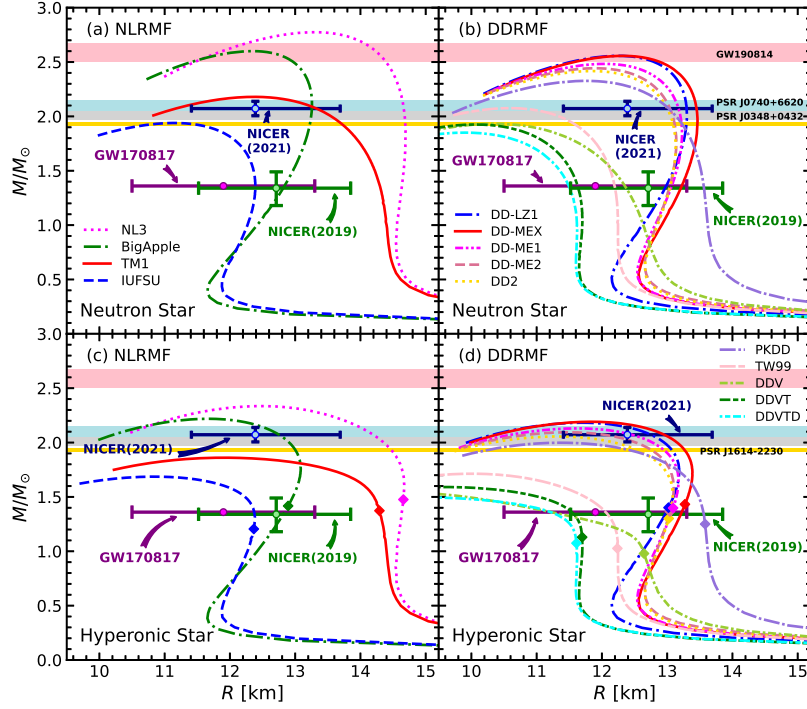


FIG. 5. The neutron and hyperonic star masses as functions of radius for NLRMF and DDRMF sets. Constraints from astronomical observables for the massive neutron star, NICER, and GW170817 are also shown. Panels (a) and panel (b) for the neutrons star matter from the NLRMF and DDRMF models, respectively. Panels (c) and panel (d) for the hyperonic star matter from the NLRMF and DDRMF models, respectively.

of symmetry energy, $L = 110.6$ MeV from TM1 and $L = 118.3$ MeV from NL3. In our previous works [138, 139], the extended TM1 and IUFSU parameter sets, which can generate different L and keep the isoscalar properties of nuclear many-body systems, were applied to systematically study the symmetry energy effect on the neutron star. We found that there is a strong correlation between the L and the radius of the neutron star at $1.4M_{\odot}$, while its influence on the maximum mass of the neutron star is very small. Furthermore, the tidal deformability, which is related to the radius of neutron also provides the constraints to L . From the present astrophysical observables, the slope of symmetry energy should be less than 80 MeV. On the other hand, L is also related to the neutron skin of the neutron-rich

nuclei, such as ^{208}Pb . However, recent experimental data about the neutron skin of ^{208}Pb from PREXII prefers the larger L [140–142]. This contradiction should be discussed in detail in the future. The softer EoSs from IUFSU, DDV, DDVT, and DDVTD cannot generate the $2M_{\odot}$ neutron stars and the radii at $1.4M_{\odot}$ from them are smaller compared to the other sets. BigApple, DD-LZ1, and DD-MEX sets can produce the neutron star heavier than $2.5M_{\odot}$, whose radii at $1.4M_{\odot}$ also accords with the constraints from gravitational wave and NICER. Therefore, we cannot exclude the possibility of the secondary in GW190814 as a neutron star [143]. For the massive neutron stars above $2M_{\odot}$, from the stiffer EoSs, their central densities are less than 0.9 fm^{-3} , while the softer EoSs may reach the central densities larger than 0.9 fm^{-3} for the lighter neutron stars.

The mass-radius ($M - R$) relations of hyperonic star from NLRMF and DDRMF parameter sets are shown in panel (c) and panel (d), respectively. The onset positions of the first hyperon in the relations are shown as the discretized symbols. After considering the strangeness degree of freedom, the maximum masses of the hyperonic star will reduce about $15\% \sim 20\%$. In the NLRMF model, only the NL3 and BigApple parameter sets can support the existence of $2M_{\odot}$ compact star with hyperons, while in the DDRMF model, the DD-LZ1, DD-MEX, DD-ME2, DD-ME1, DD2, and PKDD sets generate the hyperonic star heavier than $2M_{\odot}$. Furthermore, the central densities of the hyperonic star become higher compared to the neutron star, all of which are above $5\rho_0$. The role of hyperons in the lower mass hyperonic star is strongly dependent on the threshold density of the first onset hyperon. The properties of a hyperonic star whose central density is below this threshold are identical to those of a neutron star. When the central density of the hyperonic star is larger than the threshold, the properties of hyperonic star will be influenced. For the softer EoSs, the lower mass neutron stars are more easily affected, because their central densities are much larger than those generated by the harder EoSs at the same neutron star mass. For example, the radii of the hyperonic stars at $1.4M_{\odot}$ from DDV, DDVT, and DDVTD decrease about 5% compared to those of the neutron stars.

In Fig. (6), the dimensionless tidal deformability, Λ , of neutron stars as a function of their masses from different NLRMF and DDRMF models are shown in panel (a) and panel (b), respectively. The tidal deformability represents the quadrupole deformation of a compact star in the external gravity field generated by its companion star, which is related to the mass, radius, and Love number of the star. From the gravitation wave of BNS merger in

GW170817, it was extracted as $\Lambda_{1.4} = 190_{-120}^{+390}$ at $1.4M_{\odot}$ [18]. It is found that the $\Lambda_{1.4}$ worked out by NLRMF models are larger than the constraint of GW170817 since their radii are greater than 12 km. For the massive neutron star, its tidal deformability is very small and close to 1. The $\Lambda_{1.4}$ from DDRMF models is separated into two types. The first type with the stiffer EoSs has the larger $\Lambda_{1.4}$ and heavier masses, whose $\Lambda_{1.4}$ are out the constraint of GW170817. The second one completely satisfies the constraints of GW170817 and has smaller radii from the softer EoSs. It was also shown the tidal deformability of the neutron star at $2.0M_{\odot}$, which is expected to be measured in the future gravitational wave events from the binary neutron-star merger.

The dimensionless tidal deformabilities of hyperonic star are plotted in the panel (c) and panel (d) of Fig. (6). For the harder EoSs, the hyperons only can influence the magnitudes of Λ at the maximum star mass region, while they can reduce the dimensionless tidal deformability at $1.4M_{\odot}$ for the softer EoSs, such as TW99, DDV, DDVT, and DDVTD set, whose $\Lambda_{1.4}$ are closer to the constraints from GW170817. Therefore, the compact stars in the GW170817 events may be the hyperonic stars.

Finally, the properties of neutron star and hyperonic star, i.e., the maximum mass (M_{\max}/M_{\odot}), the corresponding radius (R_{\max}), the central density (ρ_c), the radius ($R_{1.4}$) and dimensionless tidal deformability ($\Lambda_{1.4}$) at $1.4M_{\odot}$ from present NLRMF and DDRMF models are listed in Table VI. The maximum masses of neutron stars from these models are around $1.85 \sim 2.77M_{\odot}$, whose radii are from 9.93 km to 13.32 km. The central density of heavier neutron star is smaller. It is 0.66 fm^{-3} for NL3 set, while it becomes 1.28 fm^{-3} in DDVTD set. The radius at $1.4M_{\odot}$ from DDVTD set has the smallest value, 11.46 km. Therefore, its dimensionless tidal deformability at $1.4M_{\odot}$ is just 275.

Now, the maximum masses of hyperonic stars are $1.50 \sim 2.34M_{\odot}$, and the corresponding radii are in the range of $9.30 \sim 12.51$ km, which are reduced compared to the cases without considering the strangeness degree of freedom. The central densities become larger compared to those of neutron stars. The smallest radius of the hyperonic star at $1.4M_{\odot}$ is 10.90 km from DDV, whose dimensionless tidal deformability is just 136. The threshold density of the first onset hyperon is also shown to demonstrate the influences of hyperon on the low mass hyperonic star. In general, the maximum mass of a hyperonic star can exceed $2M_{\odot}$ if the EoS is a hard type, whose maximum mass approaches $2.3M_{\odot}$ for a neutron star. Therefore, one solution to the ‘‘hyperon puzzle’’ is to adopt the stiff EoS. The softer EoS only can

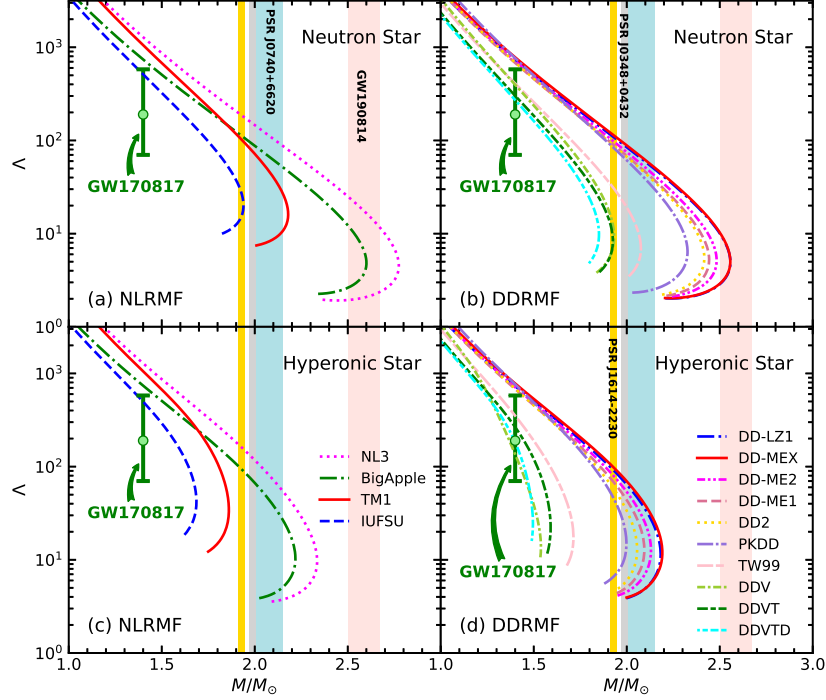


FIG. 6. The dimensionless tidal deformability as a function of star mass for NLRMF and DDRMF sets. The constraints from GW170817 event for tidal deformability is shown. Panels (a) and panel (b) for the neutrons star matter from the NLRMF and DDRMF models, respectively. Panels (c) and panel (d) for the hyperonic star matter from the NLRMF and DDRMF models, respectively.

describe the hyperonic star whose mass is around $1.5M_{\odot}$.

C. The correlations of hyperon coupling constants

In recent work, Rong *et al.* [144] found that the coupling ratio between the scalar meson and Λ hyperon, $R_{\sigma\Lambda}$, has a strong correlation with that between the vector meson and Λ hyperon, $R_{\omega\Lambda}$ in the available hypernuclei investigations by reproducing the single- Λ binding energies from relevant experiments. This correlation is easily understood in the RMF framework since the single hyperon-nucleon potential given in Eq. (33), the single hyperon-nucleon potential is dependent on the scalar field and vector one. From the present observables of Λ hypernuclei, we can extract that the $U_{\Lambda}^N \sim -30$ MeV at nuclear saturation

TABLE VI. Neutron star and hyperonic star properties from various RMF models.

	Neutron Star						Hyperonic Star						1 st threshold [fm ⁻³]
	M_{\max}/M_{\odot}	R_{\max} [km]	ρ_c [fm ⁻³]	$R_{1.4}$ [km]	$\rho_{1.4}$ [fm ⁻³]	$\Lambda_{1.4}$	M_{\max}/M_{\odot}	R_{\max} [km]	ρ_c [fm ⁻³]	$R_{1.4}$ [km]	$\rho_{1.4}$ [fm ⁻³]	$\Lambda_{1.4}$	
NL3	2.7746	13.3172	0.6638	14.6433	0.2715	1280	2.3354	12.5105	0.8129	14.6426	0.2715	1280	0.2804
BigApple	2.6005	12.3611	0.7540	12.8745	0.3295	738	2.2186	11.6981	0.8946	12.8750	0.3295	738	0.3310
TM1	2.1797	12.3769	0.8510	14.2775	0.3200	1050	1.8608	11.9255	0.9736	14.2775	0.3218	1050	0.3146
IUFSU	1.9394	11.1682	1.0170	12.3865	0.4331	510	1.6865	10.8653	1.1202	12.3520	0.4705	498	0.3800
DD-LZ1	2.5572	12.2506	0.7789	13.0185	0.3294	729	2.1824	11.6999	0.9113	12.0185	0.3294	729	0.3294
DD-MEX	2.5568	12.3347	0.7706	13.2510	0.3228	785	2.1913	11.8640	0.8890	13.2510	0.3228	785	0.3264
DD-ME2	2.4832	12.0329	0.8177	13.0920	0.3410	716	2.1303	11.6399	0.9296	13.0920	0.3410	716	0.3402
DD-ME1	2.4429	11.9085	0.8358	13.0580	0.3512	682	2.0945	11.5089	0.9560	13.0578	0.3526	681	0.3466
DD2	2.4171	11.8520	0.8481	13.0638	0.3528	686	2.0558	11.3446	0.9922	13.0630	0.3585	685	0.3387
PKDD	2.3268	11.7754	0.8823	13.5493	0.3546	758	1.9983	11.3789	1.0188	13.5400	0.3642	756	0.3264
TW99	2.0760	10.6117	1.0917	12.1805	0.4720	409	1.7135	10.0044	1.3466	11.9880	0.5710	352	0.3696
DDV	1.9319	10.3759	1.1879	12.3060	0.5035	395	1.5387	9.0109	1.7317	10.8990	0.9538	136	0.3547
DDVT	1.9253	10.0846	1.2245	11.6058	0.5458	302	1.5909	9.6244	1.4675	11.4515	0.6660	266	0.4465
DDVTD	1.8507	9.9294	1.2789	11.4615	0.5790	275	1.4956	9.3019	1.6071	10.9880	0.8570	182	0.4465

density, ρ_0 . On the other hand, the σ_0 and ω_0 are solved in the symmetry nuclear matter, which are constants. Therefore, $R_{\sigma\Lambda}$ and $R_{\omega\Lambda}$ should satisfy the linear relation, when the U_{Λ}^N is fixed in a RMF parameter set.

In this subsection, the TM1 parameter set for NN interaction will be adopted as an example to discuss the impact of the magnitudes of $R_{\sigma Y}$ and $R_{\omega Y}$ on the properties of hyperonic star under the constraints of YN potential at nuclear saturation density, $U_Y^N(\rho_0)$. From Eq. (33), we can find a linear relation between the ratios $R_{\sigma Y}$ and $R_{\omega Y}$ ($Y = \Lambda, \Sigma, \Xi$) for different hyperons. In TM1 parameter set, the magnitudes of the scalar potential, $U_S = g_{\sigma N}\sigma^0$ and the vector potential, $U_V = g_{\omega N}\omega^0$ for nucleons are 342.521 MeV and 274.085 MeV at nuclear saturation density, respectively. With the empirical hyperon-nucleon potentials for Λ , Σ and Ξ hyperons at nuclear saturation density, $U_{\Lambda}^N = -30$ MeV, $U_{\Sigma}^N = +30$ MeV and $U_{\Xi}^N = -14$ MeV, the following relations are obtained,

$$R_{\omega\Lambda} = 1.24969R_{\sigma\Lambda} - 0.10946, \quad (35)$$

$$R_{\omega\Sigma} = 1.24969R_{\sigma\Sigma} + 0.10946, \quad (36)$$

$$R_{\omega\Xi} = 1.24969R_{\sigma\Xi} - 0.05108. \quad (37)$$

Here the strange mesons σ^* and ϕ are not considered. Therefore, we can adjust the values of $R_{\omega Y}$ and generate the corresponding $R_{\sigma Y}$ simultaneously. To study the influences of $R_{\omega Y}$ on hyperonic star, $R_{\omega\Lambda}$, $R_{\omega\Xi}$, $R_{\omega\Sigma} = 0.6, 0.8, 1.0$ are discussed, respectively. Therefore, there

are 27 combination cases. The EoSs of hyperonic star matter from TM1 model with different $R_{\omega\Lambda}$, $R_{\omega\Xi}$, $R_{\omega\Sigma}$ are plotted in Fig. (7). In general, the EoS becomes stiffer with the $R_{\omega\Lambda}$ increasing. For the Σ and Ξ coupling ratios, there are also similar behaviors. It demonstrates that the vector potential increases faster than the scalar one at the high-density region so that the EoS obtains more repulsive contributions from the vector meson.

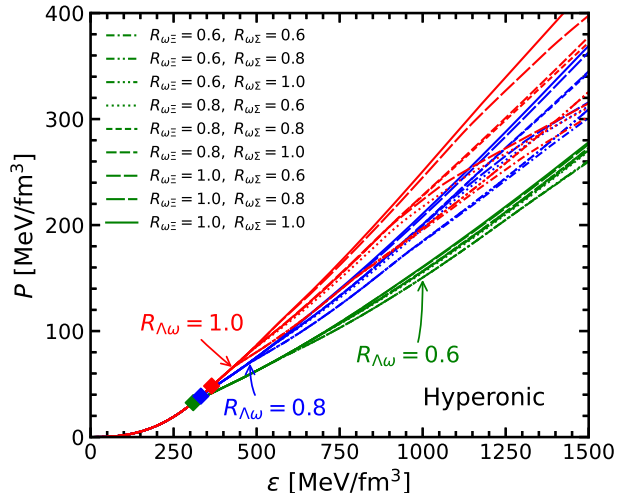


FIG. 7. The EoSs of hyperonic star matter from TM1 models with different $R_{\omega\Lambda}$, $R_{\omega\Xi}$, $R_{\omega\Sigma}$.

In Fig. (8), the pressures and speeds of sound of hyperonic star matter as functions of baryon density with different $R_{\omega\Lambda}$, $R_{\omega\Xi}$, $R_{\omega\Sigma}$ are given. The thresholds of the first hyperon onset are symbolized by the filled diamonds. When the $R_{\omega\Lambda}$ is larger, the appearances of Λ hyperons are later. Furthermore, the speeds of the sound of hyperonic matter are also strongly dependent on the magnitudes of $R_{\omega\Lambda}$, $R_{\omega\Xi}$, $R_{\omega\Sigma}$. The discontinuous places in these curves about the speeds of sound are generated by the onset of hyperons, which can reduce c_s^2 . Therefore, the speed of sound of hyperonic star matter becomes very smaller, once the types of hyperons in hyperonic stars are raised more.

In Fig. (9), the mass-radius ($M - R$) and mass-central density ($M - \rho_B$) relations from TM1 model with different $R_{\omega\Lambda}$, $R_{\omega\Xi}$, $R_{\omega\Sigma}$ are shown in panel (a) and (b), respectively. The maximum mass of neutron star from the TM1 parameter set is $2.18M_\odot$. When the hyperons are included, the maximum masses of the hyperonic star are reduced. They are just around $1.67M_\odot$ when $R_{\omega\Lambda} = 0.6$. With the increment of $R_{\omega\Lambda}$, the maximum mass of the hyperonic star becomes larger due to the stronger repulsive fields. It is around $2.0M_\odot$ in the case of

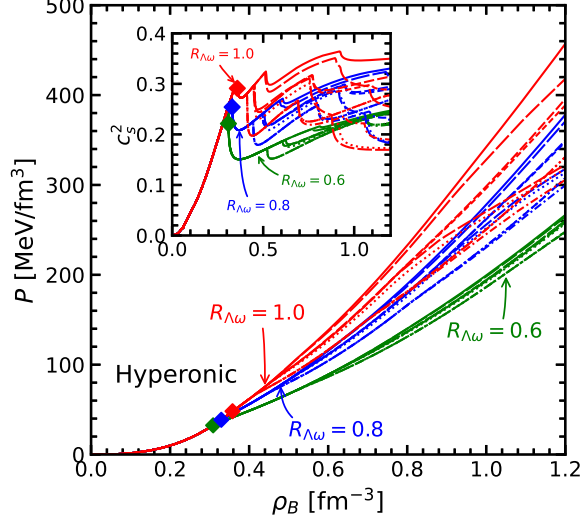


FIG. 8. The pressure of hyperonic matter as a function of baryon density with different $R_{\omega\Lambda}$, $R_{\omega\Xi}$, $R_{\omega\Sigma}$. The corresponding speeds of sound in units of the speed of light shown in sub-figure. The threshold of the first hyperon is indicated by the filled diamonds. The meaning of the curves are same as those in Fig. (7).

$R_{\omega\Lambda} = 1.0$, which satisfies the constraints from the recent massive neutron star observables. The corresponding radii turn smaller and the central densities get larger.

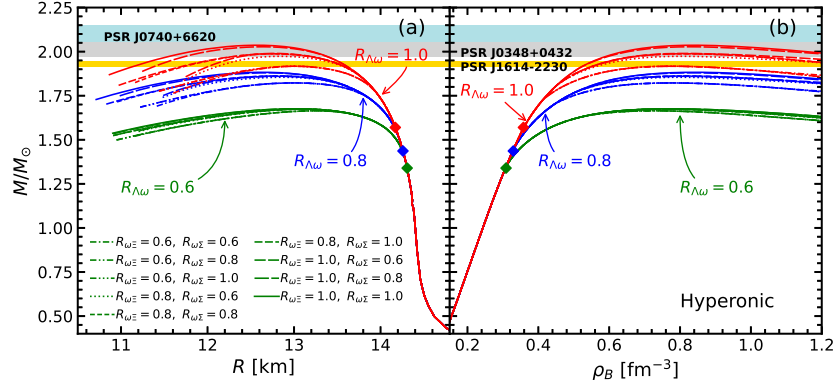


FIG. 9. The hyperonic star masses as functions of radius and the central baryon density for TM1 models with different $R_{\omega\Lambda}$, $R_{\omega\Xi}$, $R_{\omega\Sigma}$. The threshold of the first hyperon is indicated by the filled diamonds.

Finally, the thresholds of hyperons and properties of hyperonic star with different

$R_{\omega\Lambda}$, $R_{\omega\Xi}$, $R_{\omega\Sigma}$ are shown in Table.(VII). In all of these 27 cases, the Λ hyperon firstly appears in the hyperonic star. Then, if $R_{\omega\Xi} > R_{\omega\Sigma}$, the Σ^- hyperon will secondly emerge. Otherwise, the Ξ^- hyperon appears. Furthermore, when $R_{\omega\Xi} < R_{\omega\Sigma}$, the Ξ^0 can more easily arises comparing to Σ^0 and Σ^+ hyperons. The maximum masses of hyperonic star and onset density of Λ hyperon are strongly dependent on the $R_{\omega\Lambda}$ ratio. It can approach $2.04M_\odot$ when $R_{\omega\Lambda} = 1.0$, $R_{\omega\Xi} = 1.0$, $R_{\omega\Sigma} = 1.0$. The Λ hyperon appears at $\rho_B = 0.3089 \text{ fm}^{-3}$ for $R_{\omega\Lambda} = 0.6$, which is lower than the density of $1.4M_\odot$ neutron star. Therefore, the radii and dimensionless tidal deformability at $1.4M_\odot$, $R_{1.4}$ and $\Lambda_{1.4}$, are slightly changed as 12.2770 km and 1055 from the neutron star 12.2775 km and 1050. Therefore, the magnitudes of $R_{\omega\Lambda}$, $R_{\omega\Xi}$, $R_{\omega\Sigma}$ are significant to determine the maximum mass and corresponding radius of the hyperonic star, while it cannot be fixed very well through present hypernuclei experiments.

IV. SUMMARY

The neutron star consisting of nucleons and leptons, and the hyperonic star considering additional contributions from hyperons were reviewed in the relativistic mean-field (RMF) model due to recent rapid achievements about astronomical observations on the compact star. The theoretical frameworks of the two types of RMF models, i.e. non-linear RMF (NLRMF) and density-dependent RMF (DDRMF) were shown in detail to describe the infinite nuclear matter system. Several conventional NLRMF parameter sets, (NL3, BigApple, TM1, IUFSU), and the DDRMF parameter sets (DD-LZ1, DD-MEX, DD-ME2, DD-ME1, DD2, PKDD, TW99, DDV, DDVT, DDVTD) were adopted to calculate the properties of the neutron star and hyperonic star, which were created by reproducing the ground-state properties of several finite nuclei with different considerations.

The equations of state (EoSs) of neutron star matter from these parameterizations at high-density region are separated into the softer type (IUFSU, DDV, DDVT, DDVTD) and stiffer one (NL3, BigApple, TM1, DD-MEX, DD-ME2, DD-ME1, DD2, PKDD, TW99). The maximum masses of neutron stars generated by the softer EoSs cannot approach $2.0M_\odot$, which did not satisfy the constraints from the massive neutron star observables. However, the radii of the corresponding neutron star are relatively small so that their dimensionless tidal deformability at $1.4M_\odot$ are around $275 \sim 510$ which are in accord with the value

TABLE VII. Thresholds and hyperonic star properties from TM1 model with different $R_{\omega\Lambda}$, $R_{\omega\Xi}$, $R_{\omega\Sigma}$. The hyperons exist in the hyperonic star are given by bold.

$R_{\omega\Lambda}$	$R_{\omega\Xi}$	$R_{\omega\Sigma}$	Hyperon thresholds ([fm ⁻³])	M_{\max}	R_{\max} [km]	ρ_c [fm ⁻³]	$R_{1.4}$ [km]	$\rho_{1.4}$ [fm ⁻³]	$\Lambda_{1.4}$
0.6	0.6	0.6	Λ (0.3089), Ξ^- (0.5245), $\Sigma^-(0.9032)$, $\Xi^0(1.0710)$, $\Sigma^0(1.4447)$	1.6645	13.2465	0.7251	12.2770	0.3255	1055
0.6	0.6	0.8	Λ (0.3089), Ξ^- (0.5245), $\Xi^0(1.0759)$	1.6645	13.2465	0.7251	12.2770	0.3255	1055
0.6	0.6	1.0	Λ (0.3089), Ξ^- (0.5245), $\Xi^0(1.0759)$	1.6645	13.2465	0.7251	12.2770	0.3255	1055
0.6	0.8	0.6	Λ (0.3089), $\Sigma^-($ 0.6106 $)$, Ξ^- (0.6394), $\Xi^0(1.3176)$, $\Sigma^0(1.3237)$	1.6733	13.1347	0.7456	12.2770	0.3255	1055
0.6	0.8	0.8	Λ (0.3089), Ξ^- (0.6306), $\Sigma^-(1.2072)$, $\Xi^0(1.3924)$, $\Sigma^0(1.8611)$	1.6742	13.1101	0.7456	12.2770	0.3255	1055
0.6	0.8	1.0	Λ (0.3089), Ξ^- (0.6306), $\Xi^0(1.3989)$	1.6742	13.1101	0.7456	12.2770	0.3255	1055
0.6	1.0	0.6	Λ (0.3089), $\Sigma^-($ 0.6106 $)$, $\Sigma^0(1.2995)$, $\Sigma^+(1.4989)$	1.6736	13.1111	0.7514	12.2770	0.3255	1055
0.6	1.0	0.8	Λ (0.3089), $\Sigma^-(0.7830)$, $\Xi^-(0.8546)$, $\Sigma^0(1.7530)$, $\Xi^0(1.8356)$	1.6757	13.0391	0.7635	12.2770	0.3255	1055
0.6	1.0	1.0	Λ (0.3089), $\Xi^-(0.8237)$, $\Sigma^-(1.7052)$, $\Xi^0(1.8870)$	1.6757	13.0391	0.7635	12.2770	0.3255	1055
0.8	0.6	0.6	Λ (0.3294), Ξ^- (0.4485), $\Sigma^-($ 0.6979 $)$, $\Xi^0(0.8050)$, $\Sigma^0(1.0959)$	1.8225	13.0424	0.7615	12.2775	0.3200	1050
0.8	0.6	0.8	Λ (0.3294), Ξ^- (0.4485), $\Xi^0(0.8087)$	1.8225	13.0423	0.7612	12.2775	0.3200	1050
0.8	0.6	1.0	Λ (0.3294), Ξ^- (0.4485), $\Xi^0(0.8087)$	1.8225	13.0423	0.7612	12.2775	0.3200	1050
0.8	0.8	0.6	Λ (0.3294), $\Sigma^-($ 0.5009 $)$, Ξ^- (0.5150), $\Xi^0(0.9242)$, $\Sigma^0(0.9501)$	1.8547	12.8733	0.7972	12.2775	0.3200	1050
0.8	0.8	0.8	Λ (0.3294), Ξ^- (0.5103), $\Sigma^-(0.8429)$, $\Xi^0(0.9545)$, $\Sigma^0(1.3483)$	1.8619	12.7947	0.8135	12.2775	0.3200	1050
0.8	0.8	1.0	Λ (0.3294), Ξ^- (0.5103), $\Xi^0(0.9589)$	1.8619	12.7947	0.8135	12.2775	0.3200	1050
0.8	1.0	0.6	Λ (0.3294), $\Sigma^-($ 0.5009 $)$, $\Sigma^0(0.9200)$, $\Sigma^+(1.0661)$, $\Xi^-(1.1906)$	1.8603	12.8329	0.8026	12.2775	0.3200	1050
0.8	1.0	0.8	Λ (0.3294), $\Sigma^-($ 0.5967 $)$, Ξ^- (0.6220), $\Sigma^0(1.1906)$, $\Xi^0(1.2128)$	1.8799	12.6868	0.8316	12.2775	0.3200	1050
0.8	1.0	1.0	Λ (0.3294), Ξ^- (0.6135), $\Sigma^-(1.1163)$, $\Xi^0(1.2699)$, $\Sigma^0(1.8870)$	1.8828	12.6492	0.8371	12.2775	0.3200	1050
1.0	0.6	0.6	Λ (0.3579), Ξ^- (0.4186), $\Sigma^-($ 0.6050 $)$, Ξ^0 (0.6947 $)$, $\Sigma^0(0.9589)$	1.9170	13.0352	0.7661	12.2775	0.3200	1050
1.0	0.6	0.8	Λ (0.3579), Ξ^- (0.4128), Ξ^0 (0.6979 $)$, $\Sigma^-(1.4852)$, $\Sigma^0(1.5409)$	1.9174	12.9932	0.7795	12.2775	0.3200	1050
1.0	0.6	1.0	Λ (0.3579), Ξ^- (0.4128), Ξ^0 (0.6979 $)$	1.9174	12.9932	0.7795	12.2775	0.3200	1050
1.0	0.8	0.6	Λ (0.3579), $\Sigma^-($ 0.4506 $)$, Ξ^- (0.4590), Ξ^0 (0.7617 $)$, Σ^0 (0.8013 $)$	1.9736	12.8272	0.8047	12.2775	0.3200	1050
1.0	0.8	0.8	Λ (0.3579), Ξ^- (0.4548), $\Sigma^-($ 0.6947 $)$, Ξ^0 (0.7759 $)$, $\Sigma^0(1.1061)$	1.9878	12.7682	0.8093	12.2775	0.3200	1050
1.0	0.8	1.0	Λ (0.3579), Ξ^- (0.4548), Ξ^0 (0.7759 $)$	1.9879	12.7682	0.8093	12.2775	0.3200	1050
1.0	1.0	0.6	Λ (0.3579), $\Sigma^-($ 0.4506 $)$, Ξ^- (0.6726 $)$, Σ^0 (0.7617 $)$, $\Sigma^+(0.8826)$	1.9898	12.7706	0.8146	12.2775	0.3200	1050
1.0	1.0	0.8	Λ (0.3579), $\Sigma^-($ 0.5126 $)$, Ξ^- (0.5221 $)$, $\Xi^0(0.9074)$, $\Sigma^0(0.9328)$	2.0275	12.6470	0.8254	12.2775	0.3200	1050
1.0	1.0	1.0	Λ (0.3579), Ξ^- (0.5197), $\Sigma^-(0.8546)$, $\Xi^0(0.9328)$, $\Sigma^0(1.4447)$	2.0363	12.5920	0.8327	12.2775	0.3200	1050

extracted from the GW170817 event. Meanwhile, the harder EoS can lead to a very massive neutron star. The maximum masses are $2.7746M_{\odot}$ and $2.5572M_{\odot}$ from NL3 and DD-LZ1 sets, respectively, which implies that the secondary object in GW190814 may be a neutron star. In addition, the radius of the neutron star at $1.4M_{\odot}$ has a strong correlation with the slope of symmetry energy, L .

The baryon-baryon interaction plays an essential role in the hyperonic star matter, which is extracted from the experimental data of the hypernuclei. The meson-hyperon coupling strengths in RMF parameter sets were generated by the empirical hyperon-nucleon potential in symmetric nuclear matter at nuclear saturation density. The strangeness scalar and vector mesons were introduced to consider the $\Lambda - \Lambda$ potential in hyperonic star with the bond

energies of double Λ hypernuclei. The hyperonic star matter becomes softer compared to the neutron star matter. The onset densities of the first hyperon were around $2\rho_0 \sim 3\rho_0$ in present RMF models. The hyperon was raised earlier in the stiffer EoS. The appearance of hyperon can reduce the speed of the sound of the hyperonic star matter. The maximum mass of the hyperonic star is larger than $2M_\odot$ for the stiffer RMF parameter sets. In addition, the hyperons influence the properties of the hyperonic star in the low-mass region from softer EoS since its central density is very higher. Therefore, dimensionless tidal deformability at $1.4M_\odot$ will get smaller and be closer to the constraints from GW170817.

Finally, the magnitudes of the coupling strengths between scalar and vector mesons, and hyperons were discussed in the TM1 parameter set. When the single hyperon-nucleon potential in symmetric nuclear matter at nuclear saturation density was fixed at a RMF parameter set, the coupling constant between scalar meson and hyperon $R_{\sigma Y}$ has the obvious linear correlations with that between vector meson and hyperon $R_{\omega Y}$. With present hypernuclei experimental data, it is difficult to completely determine the magnitudes of $R_{\sigma Y}$ and $R_{\omega Y}$. The linear correlations were applied to investigate the effect of $R_{\omega Y}$ strength on the hyperonic star. It was found that the maximum mass of a hyperonic star can arrive at $2M_\odot$ when $R_{\omega Y} = 1.0$, while from the conventional quark counting rules, it is just around $1.7M_\odot$. Furthermore, the onset densities of various hyperons in hyperonic stars were also strongly dependent on the magnitudes of $R_{\omega Y}$. The speeds of sound of hyperonic star matter will largely reduce when the types of appearance hyperons increase.

The strangeness degree of freedom can largely affect the properties of hyperonic stars in the RMF framework and reduce the maximum mass of the hyperonic star. However, the ‘‘hyperon puzzle’’ was completely solved with the stiffer EoS generated by many available RMF parameter sets. The DDRMF models more easily generate the massive hyperonic star due to their density dependence of coupling constants. On the other hand, it is also obtained by increasing the coupling constants between the vector meson and hyperons. The gravitational wave provides a good manner to study the structure of the compact star. It is hoped that there will be special signal from gravitational waves, which can distinguish the existence of hyperons in the hyperonic star. More experiments about the hypernuclei are expected to obtain more information about the hyperon-nucleon potential, which will greatly promote the investigations about the hyperonic star.

ACKNOWLEDGMENTS

This work was supported in part by the National Natural Science Foundation of China (Grants Nos. 11775119 and 12175109) and the Natural Science Foundation of Tianjin.

- [1] N. K. Glendenning, Compact stars: Nuclear physics, particle physics and general relativity (Springer Science & Business Media, 2012). I
- [2] F. Weber, *Journal of Physics G: Nuclear and Particle Physics* **25**, R195 (1999).
- [3] M. Prakash, I. Bombaci, M. Prakash, P. J. Ellis, J. M. Lattimer, and R. Knorren, *Physics Reports* **280**, 1 (1997).
- [4] F. Weber, *Prog. Part. Nucl. Phys.* **54**, 193 (2005), astro-ph/0407155.
- [5] N. Chamel and P. Haensel, *Living Reviews in relativity* **11** (2008).
- [6] J. M. Lattimer and M. Prakash, *Physics Reports* **621**, 127 (2016).
- [7] F. Özel and P. Freire, *Annual Review of Astronomy and Astrophysics* **54**, 401 (2016).
- [8] M. Oertel, M. Hempel, T. Klähn, and S. Typel, *Rev. Mod. Phys.* **89**, 015007 (2017).
- [9] A. Li, J. Hu, S. Bao, H. Shen, and R. Xu, *Nuclear Physics Review* **36**, 1 (2019).
- [10] A. Li, Z.-Y. Zhu, E.-P. Zhou, J.-M. Dong, J.-N. Hu, and C.-J. Xia, *Journal of High Energy Astrophysics* **28**, 19 (2020). I
- [11] P. B. Demorest, T. Pennucci, S. Ransom, M. Roberts, and J. Hessels, *nature* **467**, 1081 (2010). I
- [12] E. Fonseca, T. T. Pennucci, J. A. Ellis, I. H. Stairs, D. J. Nice, S. M. Ransom, P. B. Demorest, Z. Arzoumanian, K. Crowter, T. Dolch, et al., *The Astrophysical Journal* **832**, 167 (2016).
- [13] Z. Arzoumanian, A. Brazier, S. Burke-Spolaor, S. Chamberlin, S. Chatterjee, B. Christy, J. M. Cordes, N. J. Cornish, F. Crawford, H. T. Cromartie, et al., *The Astrophysical Journal Supplement Series* **235**, 37 (2018). I
- [14] J. Antoniadis, P. C. Freire, N. Wex, T. M. Tauris, R. S. Lynch, M. H. Van Kerkwijk, M. Kramer, C. Bassa, V. S. Dhillon, T. Driebe, et al., *Science* **340**, 1233232 (2013). I
- [15] H. T. Cromartie, E. Fonseca, S. M. Ransom, P. B. Demorest, Z. Arzoumanian, H. Blumer, P. R. Brook, M. E. DeCesar, T. Dolch, J. A. Ellis, et al., *Nature Astronomy* **4**, 72 (2020). I

- [16] M. C. Miller, F. K. Lamb, A. J. Dittmann, S. Bogdanov, Z. Arzoumanian, K. C. Gendreau, S. Guillot, W. C. G. Ho, J. M. Lattimer, M. Loewenstein, et al., *The Astrophysical Journal Letters* **918**, L28 (2021). I, IIIB
- [17] B. P. Abbott, R. Abbott, T. Abbott, F. Acernese, K. Ackley, C. Adams, T. Adams, P. Addesso, R. Adhikari, V. B. Adya, et al., *Physical Review Letters* **119**, 161101 (2017). I
- [18] B. P. Abbott, R. Abbott, T. Abbott, F. Acernese, K. Ackley, C. Adams, T. Adams, P. Addesso, R. X. Adhikari, V. B. Adya, et al., *Physical Review Letters* **121**, 161101 (2018). IIIB, IIIB, IIIB
- [19] B. P. Abbott, R. Abbott, T. D. Abbott, F. Acernese, K. Ackley, C. Adams, T. Adams, P. Addesso, R. X. Adhikari, V. B. Adya, et al. (LIGO Scientific Collaboration and Virgo Collaboration), *Phys. Rev. X* **9**, 011001 (2019). I
- [20] B. P. Abbott, R. Abbott, T. D. Abbott, S. Abraham, F. Acernese, K. Ackley, C. Adams, R. X. Adhikari, V. B. Adya, et al., *The Astrophysical Journal Letters* **892**, L3 (2020). I
- [21] R. Abbott, T. D. Abbott, S. Abraham, F. Acernese, K. Ackley, C. Adams, R. X. Adhikari, V. B. Adya, C. Affeldt, M. Agathos, et al., *The Astrophysical Journal Letters* **896**, L44 (2020). I, IIIB
- [22] R. Abbott, T. D. Abbott, S. Abraham, F. Acernese, K. Ackley, A. Adams, C. Adams, R. X. Adhikari, V. B. Adya, C. Affeldt, et al., *The Astrophysical Journal Letters* **915**, L5 (2021). I
- [23] R. Abbott, T. Abbott, F. Acernese, K. Ackley, C. Adams, N. Adhikari, R. Adhikari, V. Adya, C. Affeldt, D. Agarwal, et al., arXiv preprint arXiv:2111.03606 (2021). I
- [24] I. Tews, J. Margueron, and S. Reddy, *Phys. Rev. C* **98**, 045804 (2018). I
- [25] S. De, D. Finstad, J. M. Lattimer, D. A. Brown, E. Berger, and C. M. Biwer, *Phys. Rev. Lett.* **121**, 091102 (2018).
- [26] F. J. Fattoyev, J. Piekarewicz, and C. J. Horowitz, *Phys. Rev. Lett.* **120**, 172702 (2018). I
- [27] D. G. Ravenhall, C. J. Pethick, and J. R. Wilson, *Phys. Rev. Lett.* **50**, 2066 (1983). I
- [28] R. Williams and S. Koonin, *Nuclear Physics A* **435**, 844 (1985).
- [29] K. Oyamatsu, *Nuclear Physics A* **561**, 431 (1993).
- [30] K. Oyamatsu and K. Iida, *Phys. Rev. C* **75**, 015801 (2007).
- [31] P. Magierski and P.-H. Heenen, *Phys. Rev. C* **65**, 045804 (2002).

- [32] S. S. Avancini, D. P. Menezes, M. D. Alloy, J. R. Marinelli, M. M. W. Moraes, and C. Providência, *Phys. Rev. C* **78**, 015802 (2008).
- [33] G. Watanabe, H. Sonoda, T. Maruyama, K. Sato, K. Yasuoka, and T. Ebisuzaki, *Phys. Rev. Lett.* **103**, 121101 (2009).
- [34] H. Pais and J. R. Stone, *Phys. Rev. Lett.* **109**, 151101 (2012).
- [35] A. S. Schneider, D. K. Berry, C. M. Briggs, M. E. Caplan, and C. J. Horowitz, *Phys. Rev. C* **90**, 055805 (2014).
- [36] M. E. Caplan and C. J. Horowitz, *Rev. Mod. Phys.* **89**, 041002 (2017). I
- [37] F. Grill, C. m. c. Providência, and S. S. Avancini, *Phys. Rev. C* **85**, 055808 (2012). I
- [38] S. S. Bao and H. Shen, *Phys. Rev. C* **91**, 015807 (2015). IIIB
- [39] H. Pais, S. Chiacchiera, and C. m. c. Providência, *Phys. Rev. C* **91**, 055801 (2015).
- [40] S. Yang, B. N. Zhang, and B. Y. Sun, *Phys. Rev. C* **100**, 054314 (2019).
- [41] F. Ji, J. Hu, and H. Shen, *Phys. Rev. C* **103**, 055802 (2021). I
- [42] N. K. Glendenning, *Phys. Rev. D* **46**, 1274 (1992). I
- [43] K. Schertler, S. Leupold, and J. Schaffner-Bielich, *Phys. Rev. C* **60**, 025801 (1999).
- [44] K. Schertler, C. Greiner, J. Schaffner-Bielich, and M. Thoma, *Nuclear Physics A* **677**, 463 (2000).
- [45] A. Steiner, M. Prakash, and J. Lattimer, *Physics Letters B* **486**, 239 (2000).
- [46] G. F. Burgio, M. Baldo, P. K. Sahu, and H.-J. Schulze, *Phys. Rev. C* **66**, 025802 (2002).
- [47] D. P. Menezes and C. Providência, *Phys. Rev. C* **68**, 035804 (2003).
- [48] F. Yang and H. Shen, *Phys. Rev. C* **77**, 025801 (2008).
- [49] J. Xu, L.-W. Chen, C. M. Ko, and B.-A. Li, *Phys. Rev. C* **81**, 055803 (2010).
- [50] H. Chen, G. Burgio, H.-J. Schulze, and N. Yasutake, *Astronomy & Astrophysics* **551**, A13 (2013).
- [51] M. Orsaria, H. Rodrigues, F. Weber, and G. A. Contrera, *Phys. Rev. C* **89**, 015806 (2014).
- [52] X. H. Wu and H. Shen, *Phys. Rev. C* **96**, 025802 (2017).
- [53] G. Baym, T. Hatsuda, T. Kojo, P. D. Powell, Y. Song, and T. Takatsuka, *Reports on Progress in Physics* **81**, 056902 (2018).
- [54] L. McLerran and S. Reddy, *Phys. Rev. Lett.* **122**, 122701 (2019). IIIB
- [55] X. H. Wu and H. Shen, *Phys. Rev. C* **99**, 065802 (2019).

- [56] E. Annala, T. Gorda, A. Kurkela, J. Nättilä, and A. Vuorinen, *Nature Physics* **16**, 907 (2020). III B
- [57] M. Ju, X. Wu, F. Ji, J. Hu, and H. Shen, *Phys. Rev. C* **103**, 025809 (2021).
- [58] M. Ju, J. Hu, and H. Shen, *The Astrophysical Journal* **923**, 250 (2021). I, III A
- [59] V. A. Ambartsumyan and G. S. Saakyan, *Soviet Astronomy* **4**, 187 (1960). I
- [60] N. K. Glendenning, *Physics Letters B* **114**, 392 (1982). I
- [61] N. K. Glendenning, *The Astrophysical Journal* **293**, 470 (1985). I, II C
- [62] O. Hashimoto and H. Tamura, *Progress in Particle and Nuclear Physics* **57**, 564 (2006). I
- [63] A. Feliciello and T. Nagae, *Reports on Progress in Physics* **78**, 096301 (2015).
- [64] A. Gal, E. V. Hungerford, and D. J. Millener, *Rev. Mod. Phys.* **88**, 035004 (2016).
- [65] E. Hiyama and K. Nakazawa, *Annual Review of Nuclear and Particle Science* **68**, 131 (2018). I
- [66] K. Nakazawa et al., *Nuclear Physics A* **835**, 207 (2010), proceedings of the 10th International Conference on Hypernuclear and Strange Particle Physics. I
- [67] J. K. Ahn, H. Akikawa, S. Aoki, K. Arai, S. Y. Bahk, K. M. Baik, B. Bassalleck, J. H. Chung, M. S. Chung, D. H. Davis, et al. (E373 (KEK-PS) Collaboration), *Phys. Rev. C* **88**, 014003 (2013). I
- [68] K. Nakazawa, Y. Endo, S. Fukunaga, K. Hoshino, S. Hwang, K. Imai, H. Ito, K. Itonaga, T. Kanda, M. Kawasaki, et al., *Progress of Theoretical and Experimental Physics* **2015** (2015), 033D02. I
- [69] S. H. Hayakawa, K. Agari, J. K. Ahn, T. Akaishi, Y. Akazawa, S. Ashikaga, B. Bassalleck, S. Bleser, H. Ekawa, Y. Endo, et al., *Phys. Rev. Lett.* **126**, 062501 (2021).
- [70] M. Yoshimoto, J. Ahn, B. Bassalleck, H. Ekawa, Y. Endo, M. Fujita, Y. Han, T. Hashimoto, S. Hayakawa, K. Hicks, et al., *Progress of Theoretical and Experimental Physics* **2021**, 073D02 (2021). I
- [71] E. Friedman and A. Gal, *Physics Letters B* **820**, 136555 (2021). I
- [72] J. Hu, Y. Zhang, and H. Shen, *Journal of Physics G: Nuclear and Particle Physics* **49**, 025104 (2022). I, III A
- [73] R. Knorren, M. Prakash, and P. J. Ellis, *Phys. Rev. C* **52**, 3470 (1995). I
- [74] J. Schaffner and I. N. Mishustin, *Phys. Rev. C* **53**, 1416 (1996).
- [75] H. Shen, *Phys. Rev. C* **65**, 035802 (2002). II C

- [76] R. Cavagnoli, D. P. Menezes, and C. m. c. Providência, *Phys. Rev. C* **84**, 065810 (2011).
- [77] S. Weissenborn, D. Chatterjee, and J. Schaffner-Bielich, *Phys. Rev. C* **85**, 065802 (2012).
- [78] C. m. c. Providência and A. Rabhi, *Phys. Rev. C* **87**, 055801 (2013).
- [79] S. Weissenborn, D. Chatterjee, and J. Schaffner-Bielich, *Nuclear Physics A* **914**, 421 (2013).
- [80] M. Fortin, S. S. Avancini, C. Providência, and I. Vidaña, *Phys. Rev. C* **95**, 065803 (2017).
III A, III A
- [81] Y. Zhang, J. Hu, and P. Liu, *Phys. Rev. C* **97**, 015805 (2018). I
- [82] J. J. Li, A. Sedrakian, and F. Weber, *Physics Letters B* **783**, 234 (2018).
- [83] M. Fortin, A. R. Raduta, S. Avancini, and C. m. c. Providência, *Phys. Rev. D* **101**, 034017 (2020).
- [84] W. Z. Shangguan, Z. Q. Huang, S. N. Wei, and W. Z. Jiang, *Phys. Rev. D* **104**, 063035 (2021).
- [85] Z.-H. Tu and S.-G. Zhou, *The Astrophysical Journal* **925**, 16 (2022). I
- [86] L. L. Lopes, *Communications in Theoretical Physics* **74**, 015302 (2021). I
- [87] I. Vidaña, A. Polls, A. Ramos, M. Hjorth-Jensen, and V. G. J. Stoks, *Phys. Rev. C* **61**, 025802 (2000). I
- [88] X.-R. Zhou, H.-J. Schulze, F. Pan, and J. P. Draayer, *Phys. Rev. Lett.* **95**, 051101 (2005).
- [89] H.-J. Schulze, A. Polls, A. Ramos, and I. Vidaña, *Phys. Rev. C* **73**, 058801 (2006).
- [90] H.-J. Schulze and T. Rijken, *Phys. Rev. C* **84**, 035801 (2011).
- [91] Y. Yamamoto, T. Furumoto, N. Yasutake, and T. A. Rijken, *Phys. Rev. C* **88**, 022801 (2013).
- [92] Y. Yamamoto, T. Furumoto, N. Yasutake, and T. A. Rijken, *Phys. Rev. C* **90**, 045805 (2014).
I
- [93] D. Logoteta, I. Vidana, and I. Bombaci, *The European Physical Journal A* **55** (2019). I
- [94] D. Lonardonì, A. Lovato, S. Gandolfi, and F. Pederiva, *Phys. Rev. Lett.* **114**, 092301 (2015).
I
- [95] F. Sammarruca, *Phys. Rev. C* **79**, 034301 (2009). I
- [96] T. Katayama and K. Saito, arXiv preprint arXiv:1410.7166 (2014). I
- [97] W. H. Long, B. Y. Sun, K. Hagino, and H. Sagawa, *Phys. Rev. C* **85**, 025806 (2012). I
- [98] J. Walecka, *Annals of Physics* **83**, 491 (1974). II A
- [99] J. Boguta and A. Bodmer, *Nuclear Physics A* **292**, 413 (1977). II A
- [100] B. Serot, J. Walecka, J. Negele, and E. Vogt (1986). II A

- [101] Y. Sugahara and H. Toki, Nuclear Physics A **579**, 557 (1994). II A, III A, III A, I
- [102] B. G. Todd-Rutel and J. Piekarewicz, Phys. Rev. Lett. **95**, 122501 (2005). II A
- [103] R. Brockmann and H. Toki, Phys. Rev. Lett. **68**, 3408 (1992). II A
- [104] B. A. Nikolaus, T. Hoch, and D. G. Madland, Phys. Rev. C **46**, 1757 (1992). II A
- [105] P. Ring, Progress in Particle and Nuclear Physics **37**, 193 (1996). II A
- [106] D. Vretenar, A. Afanasjev, G. Lalazissis, and P. Ring, Physics Reports **409**, 101 (2005).
- [107] J. Meng, H. Toki, S. Zhou, S. Zhang, W. Long, and L. Geng, Progress in Particle and Nuclear Physics **57**, 470 (2006).
- [108] M. Dutra, O. Lourenco, S. S. Avancini, B. V. Carlson, A. Delfino, D. P. Menezes, C. Providência, S. Typel, and J. R. Stone, Phys. Rev. C **90**, 055203 (2014). II A
- [109] B.-N. Lu, E.-G. Zhao, and S.-G. Zhou, Phys. Rev. C **84**, 014328 (2011).
- [110] Z.-X. Liu, C.-J. Xia, W.-L. Lu, Y.-X. Li, J. N. Hu, and T.-T. Sun, Phys. Rev. C **98**, 024316 (2018). II A
- [111] S. Typel, G. Röpke, T. Klähn, D. Blaschke, and H. H. Wolter, Phys. Rev. C **81**, 015803 (2010). II B, III A, II
- [112] T. Nikšić, D. Vretenar, P. Finelli, and P. Ring, Phys. Rev. C **66**, 024306 (2002). II B, III A, II
- [113] G. Lalazissis, T. Nikšić, D. Vretenar, and P. Ring, Phys. Rev. C **71**, 024312 (2005). II B, III A, III A, II
- [114] A. Taninah, S. Agbemava, A. Afanasjev, and P. Ring, Physics Letters B **800**, 135065 (2020). II B, II
- [115] W. Long, J. Meng, N. V. Giai, and S.-G. Zhou, Phys. Rev. C **69**, 034319 (2004). II B, III A, II
- [116] S. Typel and H. Wolter, Nuclear Physics A **656**, 331 (1999). II B, III A, II
- [117] S. Typel and D. Alvear Terrero, The European Physical Journal A **56** (2020). II B, III A, II
- [118] W. H. Long, B. Y. Sun, K. Hagino, and H. Sagawa, Phys. Rev. C **85**, 025806 (2012). II B, III A, II
- [119] J. R. Oppenheimer and G. M. Volkoff, Phys. Rev. **55**, 374 (1939). II C
- [120] R. C. Tolman, Phys. Rev. **55**, 364 (1939). II C
- [121] T. Hinderer, The Astrophysical Journal **697**, 964 (2009). II C
- [122] S. Postnikov, M. Prakash, and J. M. Lattimer, Phys. Rev. D **82**, 024016 (2010). II C

- [123] G. A. Lalazissis, J. König, and P. Ring, *Phys. Rev. C* **55**, 540 (1997). IIIA, IIIA, I
- [124] F. J. Fattoyev, C. J. Horowitz, J. Piekarewicz, and G. Shen, *Phys. Rev. C* **82**, 055803 (2010). IIIA, IIIA, I
- [125] F. J. Fattoyev, C. J. Horowitz, J. Piekarewicz, and B. Reed, *Phys. Rev. C* **102**, 065805 (2020). IIIA, IIIA, IIIA, I
- [126] B.-A. Li and L.-W. Chen, *Phys. Rev. C* **72**, 064611 (2005). IIIA
- [127] B.-A. Li, L.-W. Chen, and C. M. Ko, *Physics Reports* **464**, 113 (2008).
- [128] M. B. Tsang, Y. Zhang, P. Danielewicz, M. Famiano, Z. Li, W. G. Lynch, and A. W. Steiner, *Phys. Rev. Lett.* **102**, 122701 (2009).
- [129] P. Danielewicz and J. Lee, *Nuclear Physics A* **922**, 1 (2014).
- [130] M. Tsang, W. Lynch, P. Danielewicz, and C. Tsang, *Physics Letters B* **795**, 533 (2019).
- [131] B.-A. Li, P. G. Krastev, D.-H. Wen, and N.-B. Zhang, *The European Physical Journal A* **55** (2019). IIIA
- [132] P. D. Group, P. Zyla, R. Barnett, J. Beringer, O. Dahl, D. Dwyer, D. Groom, C.-J. Lin, K. Lugovsky, E. Pianori, et al., *Progress of Theoretical and Experimental Physics* **2020**, 083C01 (2020). IIIA
- [133] C. Dover and A. Gal, *Progress in Particle and Nuclear Physics* **12**, 171 (1984). IIIA
- [134] P. Khaustov, D. E. Alburger, P. D. Barnes, B. Bassalleck, A. R. Berdoz, A. Biglan, T. Bürger, D. S. Carman, R. E. Chrien, C. A. Davis, et al. (The AGS E885 Collaboration), *Phys. Rev. C* **61**, 054603 (2000). IIIA
- [135] M. C. Miller, F. K. Lamb, A. J. Dittmann, S. Bogdanov, Z. Arzoumanian, K. C. Gendreau, S. Guillot, A. K. Harding, W. C. G. Ho, J. M. Lattimer, et al., *The Astrophysical Journal* **887**, L24 (2019). IIIB
- [136] T. E. Riley, A. L. Watts, S. Bogdanov, P. S. Ray, R. M. Ludlam, S. Guillot, Z. Arzoumanian, C. L. Baker, A. V. Bilous, D. Chakrabarty, et al., *The Astrophysical Journal* **887**, L21 (2019). IIIB
- [137] T. E. Riley, A. L. Watts, P. S. Ray, S. Bogdanov, S. Guillot, S. M. Morsink, A. V. Bilous, Z. Arzoumanian, D. Choudhury, J. S. Deneva, et al., *The Astrophysical Journal Letters* **918**, L27 (2021). IIIB
- [138] F. Ji, J. Hu, S. Bao, and H. Shen, *Phys. Rev. C* **100**, 045801 (2019). IIIB

- [139] J. Hu, S. Bao, Y. Zhang, K. Nakazato, K. Sumiyoshi, and H. Shen, Progress of Theoretical and Experimental Physics **2020** (2020), 043D01. IIIB
- [140] D. Adhikari, H. Albataineh, D. Androic, K. Aniol, D. S. Armstrong, T. Averett, C. Ayerbe Gayoso, S. Barcus, V. Bellini, R. S. Beminiwattha, et al. (PREX Collaboration), Phys. Rev. Lett. **126**, 172502 (2021). IIIB
- [141] B. T. Reed, F. J. Fattoyev, C. J. Horowitz, and J. Piekarewicz, Phys. Rev. Lett. **126**, 172503 (2021).
- [142] T.-G. Yue, L.-W. Chen, Z. Zhang, and Y. Zhou, arXiv preprint arXiv:2102.05267 (2021). IIIB
- [143] K. Huang, J. Hu, Y. Zhang, and H. Shen, The Astrophysical Journal **904**, 39 (2020). IIIB
- [144] Y.-T. Rong, Z.-H. Tu, and S.-G. Zhou, Phys. Rev. C **104**, 054321 (2021). IIIC